Robust Acoustic Objective Functions and Sensitivities in Adjoint-Based Design Optimizations

Leonard V. Lopes*

NASA Langley Research Center, Hampton, Virginia, 23681

Venkat R. Iyer†

Analytical Services and Materials, Hampton, Virginia, 23681

Janelle C. Born‡

Northrop Grumman Corp., Hampton, Virginia, 23681

Abstract

The multidisciplinary design of aircraft typically includes considerations of performance, weight, fuel burn, and noise, among other factors. An objective function is applied to each of these considerations in order to weight the influence of trade-offs between different designs. Higher-order optimization exercises have utilized an adjoint approach to reach an optimal set of objective functions, such as maximum lift and reduced drag. Taking advantage of the adjoint approach significantly reduces the computational time required to find an optimal configuration. Including acoustics in the set of objective functions during an adjoint-based design optimization requires the sensitivity of the acoustic objective function. This document will present an approach for defining the sensitivity of several acoustic metrics and operations that can fill the role of the acoustic objective function. This includes time-integrated metrics such as effective perceived noise level (EPNL) and frequency-integrated metrics such as overall sound pressure level (OASPL). A demonstration case, validation, and details on the implementation in the second generation Aircraft NOise Prediction Program (ANOPP2) are also shown.

*Research Aerospace Engineer; Aeroacoustics Branch, 2 N. Dryden St, MS 461, Hampton, Virginia, 23681, Member AIAA; leonard.v.lopes@nasa.gov

†Senior Scientist; Aeroacoustics Branch, 2 N. Dryden St, MS 461, Hampton, Virginia, 23681, venkat.r.iyer@nasa.gov

‡Computer Progammer; Aeroacoustics Branch, 2 N. Dryden St, MS 461, Hampton, Virginia, 23681, janelle.c.born@nasa.gov

I. Introduction

The NASA Aeronautics Research Mission Directorate continues to push the bounds of current aircraft technology by motivating the aircraft community, both internal and external to NASA, to design aircraft that meet increasingly challenging goals[1, 2]. Toward that end, the NASA Advanced Air Vehicles Program (AAVP), Integrated Aviation Systems Program (IASP), and Transformative Aeronautics Concepts Program (TACP) include multidisciplinary efforts to cultivate new technologies and mature existing technologies from conceptual design to the current airspace system. Projects such as the Transformational Tools and Technologies (TTT) of TACP and the Revolutionary Vertical Lift Technology (RVLT) of AAVP focus on developing new computer-based tools, models, and knowledge that provide a first-of-a-kind capability to analyze and predict performance of new aircraft concepts. This includes bringing computer-aided design techniques and Computational Fluid Dynamics (CFD) to the forefront of the aircraft design process, including taking advantage of gradient-based optimization frameworks such as Phoenix Integration's ModelCenter® or OpenMDAO[3] developed at NASA.

Aircraft design and optimization include many design variables, such as aircraft geometric properties, flight path details, and engine properties, but typically only a few objective functions, such as weight, fuel burn, and noise. In gradient-based design approaches, one of the major challenges is to provide the sensitivity of the objective functions with respect to all of the design variables. Various approaches are available to determine the sensitivities[4], including finite differencing, complex differentiation, and adjoint techniques. Even though there have been major inroads in reducing the computation time required to achieve an adequate unsteady flow solution, finite differencing and complex differentiation techniques still require many flow solves in order to provide the sensitivity of the objective functions for all design variables. Adjoint methodology has gained traction for a variety of problems since it maps the entire design space in a single computation. This is attractive when there are a large number of design variables and few objective functions. Recently, there has been a push to apply the adjoint technique to CFD, allowing for CFD-driven, adjoint-based design optimizations[5]. With increasing computational power, adjoint-based optimizations with time-dependent flow calculations are becoming more routine; however, to date, there has been little effort to include a realistic acoustic objective function in adjoint optimizations, such as that required for aircraft noise certification.

In the adjoint approach, the sensitivities of an objective function are determined through a solution of an auxiliary, or adjoint, set of equations. The principal advantage of the adjoint technique is that the computational cost is independent of the number of design variables; that is, a sensitivity analysis for thousands of design variables can be performed at a cost equivalent to the solution of the governing equations themselves. As a result, multidisciplinary design optimization that minimizes a realistic aircraft

noise certification metric can be achieved once the sensitivity of the noise metric is defined. I For most noise predictions, in addition to computing/estimating the source strength, there are two acoustic calculations that must occur. The first is the propagation of noise, such as 1/3-octave band sound pressure level (SPL) spectra or acoustic pressure time histories (APTH), from the source region to the observer location. The second is the calculation of a derived acoustic metric, such as effective perceived noise level (EPNL). In this paper, an approach using analytic differentiation (ND) is presented to determine the sensitivity of many common derived acoustic metrics, including those that would be required in aircraft noise certification.[a] The sensitivities are implemented as part of the NASA second generation Aircraft NOise Prediction Program (ANOPP2)[6, 7]. Also, no source code transformation (automatic differentiation) tool has been applied; all derivatives have been implemented and validated within ANOPP2 by hand. Validation of the sensitivity of the acoustic metric is performed by comparing the sensitivity to that calculated by the finite differencing (FD) and complex differentiation (CD) approaches. An example case is shown that uses the sensitivities of multiple acoustic metrics to compute the optimal exposure area on a grid of observers placed below a monopole source.

II. Acoustic Objective Function

The first part of this paper addresses a realistic acoustic objective function in adjoint-based, CFD-driven noise computations. However, although it is not explicitly presented here, this work can also be applied to any noise research area where sensitivity of derived acoustic metrics is required, such as aircraft design using semiempirical methods.

Using the node-centered discretization approach outlined in Reference 8, the flow solution can be represented by

$$\frac{\partial(\mathbf{Q}V)}{\partial t} + \mathbf{R} = 0, \qquad \mathbf{R} \equiv \oint_{\partial V} (\mathbf{F}_i - \mathbf{F}_v) \cdot \hat{\mathbf{n}} \mathrm{d}S \tag{1}$$

where t is time, V is the control volume bounded by ∂V, $\mathbf{Q}$ represents the volume-averaged conservative variables, $\mathbf{R}$ is the spatially undivided residual at each control volume, S is the control volume surface area, $\hat{\mathbf{n}}$ is the outward pointing normal vector, and $\mathbf{F}_i$ and $\mathbf{F}_v$ denote the inviscid and viscous fluxes, respectively. The time-derivative in Eq. 1 can be discretized any number of ways. For the purpose of this study, only first-order backward difference (BDF1) is shown. This is shown for time-level n as follows:

$$\mathbf{V}^n \frac{\mathbf{Q}^n - \mathbf{Q}^{n-1}}{\Delta t} + \mathbf{R}^n + \mathbf{R}^n_{GCL}\mathbf{Q}^{n-1} = 0 \tag{2}$$

[a]Abbreviation 'ND' is used in place of 'AD' which is commonly used for automatic differentiation (a.k.a. algorithmic differentiation).

where the residual of the geometric conservation law (GCL) is included by way of $\mathbf{R}_{\mathrm{GCL}}$[9].

The adjoint-based optimization methodology is based on the method of Lagrange multipliers. The goal is to compute the sensitivity of an objective function, $\mathscr{F}$, with respect to design variables, $\mathbf{D}$, subject to the constraint of Eq. 2. For the time-dependent equations that include dynamic grids, the Lagrangian functional, L, can be defined as

$$L = \mathscr{F} + \sum_{n=1}^{N} [\mathbf{\Lambda}_f^n]^T \left(\mathbf{V}^n \frac{\mathbf{Q}^n - \mathbf{Q}^{n-1}}{\Delta t} + \mathbf{R}^n + \mathbf{R}_{\mathrm{GCL}}^n \mathbf{Q}^{n-1} \right) \Delta t + \sum_{n=1}^{N} [\mathbf{\Lambda}_g^n]^T \mathbf{G}^n \Delta t + [\mathbf{\Lambda}_f^0]^T \mathbf{R}^{in} \Delta t + [\mathbf{\Lambda}_g^0]^T \mathbf{G}^0 \Delta t \quad (3)$$

where $\mathbf{G}$ is a grid operator and is a function of the node positions $\mathbf{X}$[10]. $\mathbf{\Lambda}_f$ and $\mathbf{\Lambda}_g$ are adjoint vectors associated with the flow and grid equations, respectively. Superscript n denotes the time level, T denotes a transpose operation, in denotes initial condition, and Δt is the time step size. Many of the details in the derivation of the Lagrangian are left out for brevity; see References 5 and 11 for more information.

Equation 3 is differentiated with respect to the design variables. Regrouping terms to isolate the coefficients of $d\mathbf{Q}^n/d\mathbf{D}$ and $d\mathbf{X}^n/d\mathbf{D}$ and equating the coefficients to zero results in the following set of adjoint equations (Eq. 4 through Eq. 9). Once a flow solution is determined, Eqs. 4 through 9 can be solved in reverse time to determine the set of adjoint vectors.

For $N = n$,

$$\frac{1}{\Delta t} \mathbf{V}^N \mathbf{\Lambda}_f^N + \left[\frac{\partial \mathbf{R}^N}{\partial \mathbf{Q}^N} \right]^T \mathbf{\Lambda}_f^N = - \left[\frac{\partial \mathscr{F}}{\partial \mathbf{Q}^N} \right]^T \quad (4)$$

$$- \left[\frac{\partial \mathbf{G}^N}{\partial \mathbf{X}^N} \right]^T \mathbf{\Lambda}_g^N = \left[\frac{\partial \mathscr{F}}{\partial \mathbf{X}^N} \right]^T + \left[\frac{\partial \mathbf{V}^N}{\partial \mathbf{X}^N} \frac{\mathbf{Q}^N - \mathbf{Q}^{N-1}}{\Delta t} \right]^T \mathbf{\Lambda}_f^N + \left[\frac{\partial \mathbf{R}^N}{\partial \mathbf{X}^N} + \frac{\partial \mathbf{R}_{\mathrm{GCL}}^N}{\partial \mathbf{X}^N} \mathbf{Q}^{N-1} \right]^T \mathbf{\Lambda}_f^N \quad (5)$$

For $N > n \geq 1$,

$$\frac{1}{\Delta t} \left(\mathbf{V}^n \mathbf{\Lambda}_f^n - \mathbf{V}^{n+1} \mathbf{\Lambda}_f^{n+1} \right) + \left[\frac{\partial \mathbf{R}^n}{\partial \mathbf{Q}^n} \right]^T \mathbf{\Lambda}_f^n + \left[\mathbf{R}_{\mathrm{GCL}}^{n+1} \right]^T \mathbf{\Lambda}_f^{n+1} = - \left[\frac{\partial \mathscr{F}}{\partial \mathbf{Q}^n} \right]^T \quad (6)$$

$$- \left[\frac{\partial \mathbf{G}^n}{\partial \mathbf{X}^n} \right]^T \mathbf{\Lambda}_g^n = \left[\frac{\partial \mathscr{F}}{\partial \mathbf{X}^n} \right]^T + \left[\frac{\partial \mathbf{V}^n}{\partial \mathbf{X}^n} \frac{\mathbf{Q}^n - \mathbf{Q}^{n-1}}{\Delta t} \right]^T \mathbf{\Lambda}_f^n + \sum_{k=0}^{1} \left[\frac{\partial \mathbf{R}^{n+k}}{\partial \mathbf{X}^n} + \frac{\partial \mathbf{R}_{\mathrm{GCL}}^{n+k}}{\partial \mathbf{X}^n} \mathbf{Q}^{n+k-1} \right]^T \mathbf{\Lambda}_f^{n+k} \quad (7)$$

For $n = 0$,

$$- \frac{1}{\Delta t} \mathbf{V}^1 \mathbf{\Lambda}_f^1 + \left[\frac{\partial \mathbf{R}^{in}}{\partial \mathbf{Q}^0} \right]^T \mathbf{\Lambda}_f^0 + \left[\mathbf{R}_{\mathrm{GCL}}^1 \right]^T \mathbf{\Lambda}_f^1 = - \left[\frac{\partial \mathscr{F}}{\partial \mathbf{Q}^0} \right]^T \quad (8)$$

$$- \left[\frac{\partial \mathbf{G}^0}{\partial \mathbf{X}^0} \right]^T \mathbf{\Lambda}_g^0 = \sum_{n=1}^{N} \left[\frac{\partial \mathbf{G}^n}{\partial \mathbf{X}^0} \right]^T \mathbf{\Lambda}_g^n + \left[\frac{\partial \mathscr{F}}{\partial \mathbf{X}^0} \right]^T + \left[\frac{\partial \mathbf{R}^{in}}{\partial \mathbf{X}^0} \right]^T \mathbf{\Lambda}_f^0 + \left[\frac{\partial \mathbf{R}^1}{\partial \mathbf{X}^0} + \frac{\partial \mathbf{R}_{\mathrm{GCL}}^1}{\partial \mathbf{X}^0} \mathbf{Q}^0 \right]^T \mathbf{\Lambda}_f^1 \quad (9)$$

Once the adjoint vectors are known, Eq. 10 is used to determine the sensitivity of the Lagrangian with

respect to the design variables.

$$\frac{\mathrm{d}L}{\mathrm{d}\mathbf{D}} = \frac{\partial \mathscr{F}}{\partial \mathbf{D}} + \sum_{n=1}^{N} \left([\mathbf{\Lambda}_f^n]^T \left[\frac{\partial \mathbf{R}^n}{\partial \mathbf{D}} + \frac{\partial \mathbf{R}_{\mathrm{GCL}}^n}{\partial \mathbf{D}} \mathbf{Q}^{n-1} \right] + [\mathbf{\Lambda}_g^n]^T \frac{\partial \mathbf{G}^n}{\partial \mathbf{D}} \right) \Delta t + \left([\mathbf{\Lambda}_f^0]^T \frac{\partial \mathbf{R}^{in}}{\partial \mathbf{D}} + [\mathbf{\Lambda}_g^0]^T \frac{\partial \mathbf{G}^0}{\partial \mathbf{D}} \right) \Delta t \quad (10)$$

After solving Eq. 10, an optimization technique, such as the method of steepest descent, can then be utilized to find the maximum or minimum of the objective function by iteratively setting the design variables using the previous set of design variables and the sensitivity of the Lagrangian of the objective function.

III. Sensitivity of Common Acoustic Metrics

The sensitivity of the Lagrangian, shown in Eq. 10, requires solving for the adjoint vectors, $\mathbf{\Lambda}_g$ and $\mathbf{\Lambda}_f$, using the adjoint equations, Eqs. 4 through 9. FUN3D[12] can provide the sensitivities of the flow solution, flow residual, and grid operators; therefore, the only unknowns are the sensitivity of the acoustic objective function, $\mathscr{F}$, to the flow solution, $\mathbf{Q}$, grid coordinates, $\mathbf{X}$, and design variable, $\mathbf{D}$. The acoustic objective function, in general, will not be directly relatable to the design variables; therefore, the partial derivative of the objective function with respect to the design variable is zero.[b]

$$\frac{\partial \mathscr{F}}{\partial \mathbf{D}} = 0 \quad (11)$$

The sensitivities of the acoustic objective function with respect to the flow solution and grid operator can be expanded using the chain rule, shown in Eq. 12, where $\mathbf{M}$ is any acoustic metric that may be predicted at the observer, such as an APTH or a time history of 1/3-octave band SPL spectra. This operation separates the problem into two components: the sensitivity of acoustic objective function to the acoustic metric at the observer and the sensitivity of the acoustic metric at the observer to the definition of the noise source; in the current effort, the flow solution and grid coordinates.

$$\frac{\partial \mathscr{F}}{\partial \mathbf{Q}^n} = \frac{\partial \mathscr{F}}{\partial \mathbf{M}} \frac{\partial \mathbf{M}}{\partial \mathbf{Q}^n}, \qquad \frac{\partial \mathscr{F}}{\partial \mathbf{X}^n} = \frac{\partial \mathscr{F}}{\partial \mathbf{M}} \frac{\partial \mathbf{M}}{\partial \mathbf{X}^n} \quad (12)$$

The sensitivities of the acoustic objective function with respect to the flow solution and the grid operator contain a common component, the sensitivity of the acoustic objective function with respect to the acoustic metric at the observer ($\frac{\partial \mathscr{F}}{\partial \mathbf{M}}$). The sensitivity of the acoustic objective function to the acoustic metric at the observer is the focus of this study. The sensitivities of the acoustic metric at the observer with respect to the flow solution ($\frac{\partial \mathbf{M}}{\partial \mathbf{Q}^n}$) and the grid operator ($\frac{\partial \mathbf{M}}{\partial \mathbf{X}^n}$) are the focus of follow on work.

[b] An acoustic objective function may include lateral (sideline) observer position that is placed relative to the aircraft's altitude during takeoff, which, in turn, may be a function of the design variable. This dependency will not be addressed in this study, but can be addressed via chain rule and the pressure gradient formulation (Formulation G1A[13]) as such: $\frac{\partial \mathscr{F}}{\partial \mathbf{D}} = \frac{\partial \mathscr{F}}{\partial \mathbf{p}} \frac{\partial \mathbf{p}}{\partial \mathbf{x}} \frac{\partial \mathbf{x}}{\partial \mathbf{D}}$ where $\mathbf{x}$ is the observer position and $\mathbf{p}$ is the APTH at the observer.

Up to this point, the acoustic objective function and acoustic metric at the observer have not been defined because many combinations are possible, and the desired objective function and acoustic metric at the observer are application dependent. Examples of acoustic objective functions include those that are required for noise certification, such as EPNL or sound exposure level (SEL), and examples of acoustic metric at the observer include an APTH or a time history of 1/3-octave band SPL spectra. Some combinations may require significantly less computational effort than others. The available metrics in ANOPP2[6, 7] are shown in Fig. 1 and serve to provide a guideline for the sensitivities required for the majority of applications.[c] The sensitivity of the acoustic objective function with respect to the metric at the observer can be found by use of common acoustic analysis operations. For example, if the acoustic objective function is EPNL and acoustic metric at the observer is an APTH, then the metrics that are required are shown in Eq. 13.

$$\begin{aligned} \mathscr{F} = \mathrm{EPNL} = f(\mathbf{PNLT}), \qquad \mathrm{PNLT}_j = f(\mathbf{L}_{\mathrm{B},j}), \qquad \mathrm{L}_{\mathrm{B},b,j} = f(\boldsymbol{G}_{pp,j}), \qquad G_{pp,m,j} = f(\boldsymbol{p}_{w,j}), \\ p_{n,w,j} = f(\boldsymbol{p}_j), \qquad p_{n',j} = f(\boldsymbol{p}) \end{aligned} \tag{13}$$

where subscript j represents a single short duration interval (typically 0.5 seconds) of the entire long duration time history, subscript b represents each band in the 1/3-octave band SPL spectrum ($\mathrm{L_B}$), subscript m is each bin in the power spectral density (PSD) G_{pp}, subscript w is a windowed APTH, and n and n' represent each time step in the short duration APTH. The vector of PNLT values is sized by the number of short intervals; $\mathrm{L_B}$ is sized by 24 for the standard 1/3-octave center band frequencies ranging from 50 to 10,000 Hz; the PSD is sized by the number of frequency bins; the windowed and nonwindowed short duration APTH are sized by the number of reception time steps within one interval; and the long duration APTH is sized by the total number of reception times. The sensitivity of EPNL with respect to the long duration APTH requires the following six sensitivities.

$$\frac{\partial \mathrm{EPNL}}{\partial \mathbf{PNLT}}, \qquad \frac{\partial \mathrm{PNLT}_j}{\partial \mathbf{L}_{\mathrm{B},j}}, \qquad \frac{\partial \mathrm{L}_{\mathrm{B},b,j}}{\partial \boldsymbol{G}_{pp,j}}, \qquad \frac{\partial G_{pp,m,j}}{\partial \boldsymbol{p}_{w,j}}, \qquad \frac{\partial \boldsymbol{p}_{w,j}}{\partial \boldsymbol{p}_j}, \qquad \frac{\partial \boldsymbol{p}_j}{\partial \boldsymbol{p}} \tag{14}$$

If OASPL is the acoustic objective function, a much shorter APTH requirement removes the operation of creating intervals because the analysis requires only a short duration APTH. A similar analysis as above results in the required four sensitivities shown in Eq. 15.

$$\frac{\partial \mathrm{L}_A}{\partial \boldsymbol{G}_{pp,\mathrm{A}}}, \qquad \frac{\partial G_{pp,\mathrm{A},m'}}{\partial \boldsymbol{G}_{pp}}, \qquad \frac{\partial G_{pp,m}}{\partial \boldsymbol{p}_w}, \qquad \frac{\partial \boldsymbol{p}_w}{\partial \boldsymbol{p}} \tag{15}$$

where L is the OASPL, subscript A denotes A-weighted value (although no weighting is necessary), and m'

[c] Several other operations are also available in the Acoustic Analysis API of ANOPP2 but are not presented here. These include unit conversion capabilities and combining several available acoustic metrics of different resolution and bounds.

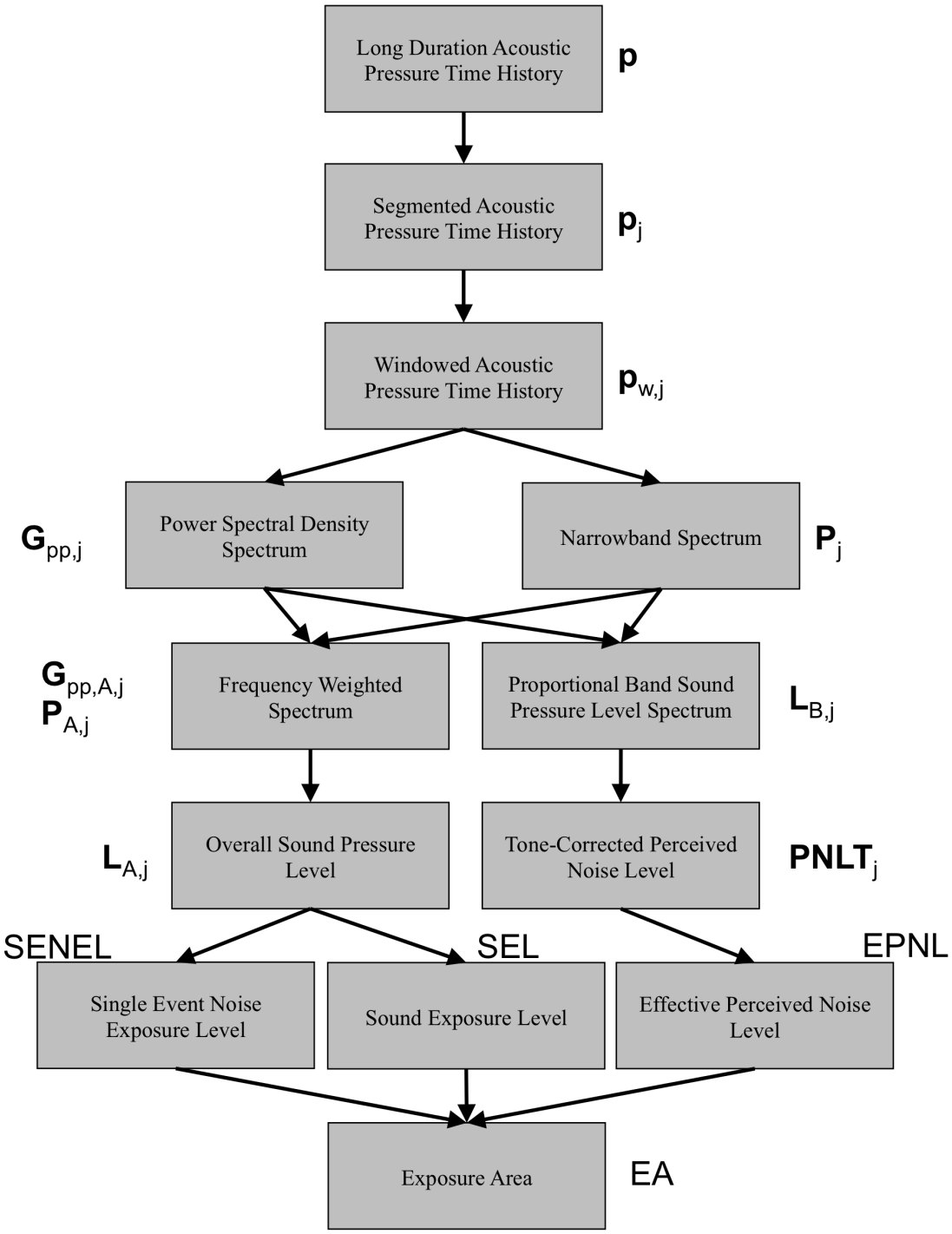

Figure 1. A flow chart of available acoustic metrics within ANOPP2.

is each bin in the A-weighted PSD.

Since the choice of starting metric and objective function can be any number of combinations, it is easier to define the sensitivity of each metric with respect to its inputs individually and leave the choice, evaluation, and multiplication order up to the application. The next part of the current study presents the sensitivity of each acoustic metric to the inputs required to compute it, but not before a brief discussion on the validation approach.

Validation

The ND sensitivities of all available acoustic metrics in ANOPP2 are validated by comparing to the sensitivity found by using the CD and FD (second order central) approaches. Two validation approaches are required because the implementation of the CD approach in ANOPP2, although only used to validate the ND approach, is a new capability and requires validation itself. The sensitivities using the FD approach are found by calculating the metric twice using slightly different input; if the metric is a function of a list of inputs, such as every time step in an APTH, the metric is calculated twice for every input in the list, first for the input plus Δ, then again with the input minus Δ. The second order central difference is shown in Eq. 16. The sensitivity using the CD approach is found by converting all real values in ANOPP2 to complex values and perturbing an input in the complex plane by ϵ. Eq. 17 is then used to determine the sensitivity. Similar to finite differencing, the complex form of the metric calculation is computed once for every input. Sensitivities calculated using the CD approach are much more accurate due to the feasibility of very small perturbations, $\epsilon \approx 10^{-10}$. A study was performed (not shown here) on the value of the perturbations used in both the FD and ND approach; the results were found to be relatively insensitive to both Δ and ϵ. Only one execution of the ND approach is required, as all sensitivities are determined at once; as a result, the ND approach is not only extremely accurate but also very fast compared to FD and CD approaches. The sensitivities of the acoustic metric calculated using the ND approach require a computation time on the order of the calculation of the metric while sensitivities of the acoustic metric using the CD and FD approaches require a computation time on the order of the calculation of the metric times the number of inputs. For each metric, two total relative errors are calculated, one between the sensitivities calculated using the ND and FD approaches and one between the ND and CD approaches.

$$\frac{\partial F}{\partial x} = \frac{F(x+\Delta) - F(x-\Delta)}{2\Delta} + \mathrm{O}(\Delta^2) \tag{16}$$

$$\frac{\partial F}{\partial x} = \frac{\mathrm{Im}(F(x+i\epsilon))}{\epsilon} + \mathrm{O}(\epsilon^2) \tag{17}$$

A. Segmentation

Segmentation is the operation of extracting a subset of the long duration APTH into a shorter segment for frequency analysis. The analytic sensitivity of the segmenting algorithm is simple and is shown in Eq. 18, where $\boldsymbol{p}_j$ is the jth segment, n is the nth time step of the segmented APTH, and n' is the n'th time step of the long duration APTH. Due to its simplicity, validation of the segmentation calculation is not shown here.

$$\frac{\partial p_{j,n}}{\partial p'_n} = \delta_{n,n'} \tag{18}$$

B. Windowing

The discrete Fourier transform assumes an infinitely repeatable signal of finite period; this may lead to high frequency error unless care is taken to remove the discontinuities during transition between signals. Windows often are applied to an APTH (either long or short duration) to 'smooth' out the function near the transition. Common windowing functions include Rectangular, Hanning, Hamming, Flat Top, and Blackman[14]. Equation 19 shows the windowing function, where p_n is the unwindowed long or short duration APTH, $p_{n,w}$ is the windowed long or short duration APTH, w_n is the windowing function, and A_w is the scaling factor of the windowing function. Also shown in Eq. 19 is the ND of the windowing operation.

$$p_{n,w} = \sqrt{A_w} w_n p_n, \qquad \frac{\partial p_{w,n}}{\partial p'_n} = \sqrt{A_w} w_n \delta_{n,n'} \qquad \text{where} \qquad A_w = N \sum_{n=0}^{N-1} w_n^{-2} \tag{19}$$

Figure 2 shows a comparison between the sensitivities calculated by the FD, CD, and ND approaches shown in Eq. 19 with a Hanning window function. The APTH used as input to the validation was composed of a single sinusoid of ten periods, one thousand time steps, and an amplitude of one Pa, shown in Fig 2a). The perturbation values for the CD and FD approaches were ϵ of 10^{-10} Pa and Δ of 1% of the amplitude of the sine wave, respectively. The total percent error between sensitivities calculated using the ND and FD approaches was 7.795×10^{-14}% and between the sensitivities calculated using the ND and CD approaches was 1.736×10^{-15}%. As expected, the sensitivities calculated using the ND and CD approaches were much closer than between the ND and FD approaches due to numerical inaccuracies in the finite differencing of the FD approach. This is a common theme throughout this effort.

C. Filtered Acoustic Pressure Time History

It is often desirable to focus on an APTH that contains a certain subset of all possible frequencies. This is accomplished through a filtering operation defined by a high and low pass filter frequency, f_{hp} and f_{lp}, respectively. A filtered APTH is found by first performing a discrete Fourier transform to calculate a set

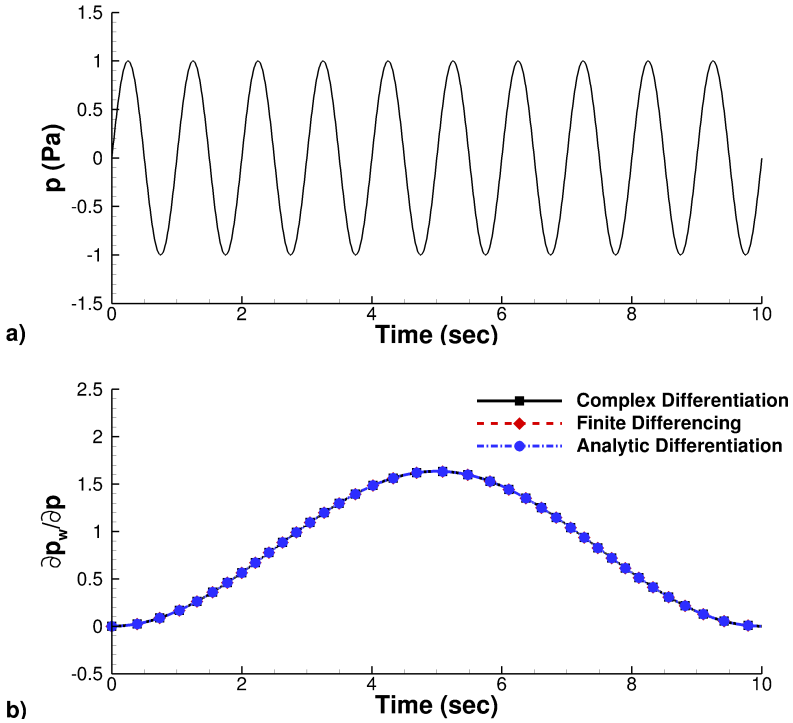

Figure 2. a) Representative APTH. b) Sensitivity of windowed APTH with respect to unwindowed APTH using CD, FD, and ND.

of Fourier coefficients shown in Eq. 20, where p_n is an APTH of N samples. An inverse Fourier transform is performed using only the Fourier coefficients that match the criteria set by the high and low pass filter frequency, $A_{m,f}$, shown in Eq. 21.

$$A_m = \sum_{n=0}^{N} p_n e^{-2\pi i n m/N} \tag{20}$$

$$p_{n,f} = \frac{1}{N}\sum_{m=0}^{N-1} A_{m,f} e^{2\pi i n m/N} \qquad \text{where} \qquad A_{m,f} = \begin{cases} A_m & f_{hp} \le f_m \le f_{lp} \\ 0 & f_{hp} > f_m \text{ or } f_m > f_{lp} \end{cases} \tag{21}$$

The sensitivity of this operation can be found symbolically by differentiating the above equations. The symbolic differentiation is shown in the following equation where L is defined as the set of indices excluded by the filtering operation.

$$\frac{\partial p_{f,n}}{\partial p_{n'}} = \frac{\partial}{\partial p_{n'}}\left\{\frac{1}{N}\sum_{m=0}^{N-1} A_{m,f} e^{2\pi i n m/N}\right\} = \frac{1}{N}\frac{\partial}{\partial p_{n'}}\left\{\sum_{m=0}^{N-1} A_m e^{2\pi i n m/N} - \sum_{l\in L} A_l e^{2\pi i n l/N}\right\} \tag{22}$$

This is then easily simplified by placing Eq. 20 into Eq. 22.

$$\frac{\partial p_{f,n}}{\partial p_{n'}} = \delta_{nn'} - \frac{1}{N}\sum_{l\in L}\frac{\partial A_l}{\partial p_{n'}} e^{2\pi i n l/N} = \delta_{nn'} - \frac{1}{N}\sum_{l\in L} e^{2\pi i l(n-n')/N} \tag{23}$$

As an example of the sensitivity of the filtering operation, an APTH is constructed of 3 sinusoids of amplitude 1 Pa, frequencies of 1, 4, and 12 Hz, and phase offsets of 0, $\pi/4$, and $\pi/2$ radians. The high and low pass filter frequencies are set such that the 1 and 12 Hz content is removed. The unfiltered and filtered APTH are shown in Fig. 3. Figure 4 shows the sensitivity of the filtered APTH with respect to the unfiltered APTH using the FD, CD, and ND approaches. The perturbation values for the CD and FD approaches were ϵ of 10^{-10} Pa and Δ of 1% of the maximum amplitude of the unfiltered APTH, respectively. The relative error between the ND and FD approaches was 4.562×10^{-10}% and between the ND and CD approaches was 6.3270×10^{-14}%. As expected, numerical issues contaminate the FD approach, leading to a higher relative error when compared to the CD and ND approaches.

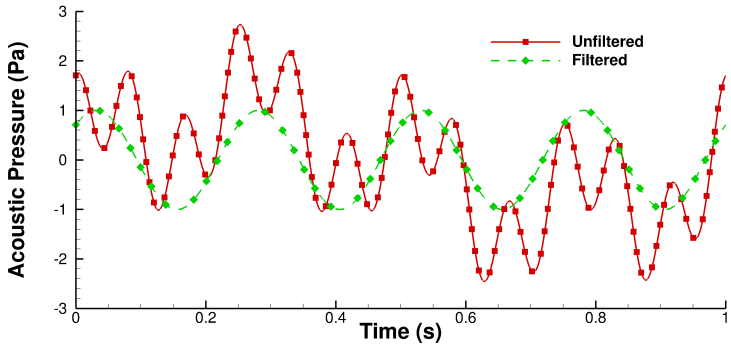

Figure 3. Representative APTH composed of 3 sinusoids and filtered APTH where the higher and lower frequency content is removed.

D. Power Spectral Density and Narrowband Spectra

Acoustic analysis often involves the calculation of derived noise metrics as a function of frequency rather than of time. Acoustic measurements and calculations often are performed in the time domain and need to be converted to the frequency domain for analysis. The Fourier transform is used to convert a time domain acoustic signal to a frequency domain spectrum, either a PSD or a narrowband spectrum. The derivation for the sensitivity of the narrowband spectrum is similar to the sensitivity of the PSD and will not be explicitly shown here. The PSD is calculated from an APTH via the complex Fourier coefficients, shown in Eq. 24 and Eq. 25, where G_{pp} is the PSD, T is the period of the APTH, N is the number of samples in the APTH, m is the mth bin in the PSD, and A_m are complex Fourier coefficients, which are calculated from the APTH, shown in Eq. 20.

$$G_{pp,m} = \frac{|A_m|^2 T}{N^2} \quad \text{for} \quad m = 0 \tag{24}$$

$$G_{pp,m} = 2\frac{|A_m|^2 T}{N^2} \quad \text{for} \quad 1 \leq m \leq \frac{N}{2} - 1 \tag{25}$$

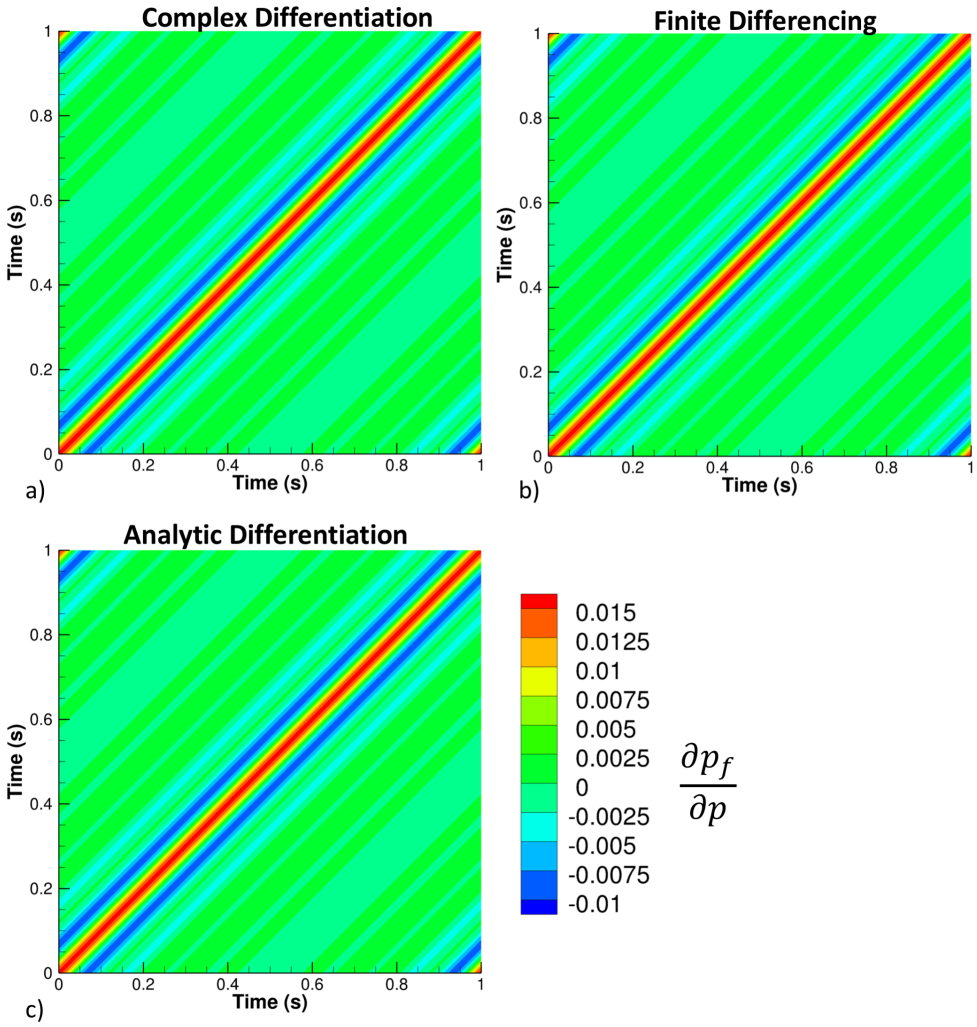

Figure 4. Sensitivity of filtered APTH with respect to unfiltered APTH using a) CD, b) FD, and c) ND.

The sensitivity of the PSD with respect to the windowed APTH using ND is shown in Eq. 26 and 27.

$$\frac{\partial G_{pp,m}}{\partial \boldsymbol{p}_w} = 2\frac{T}{N^2}\left\{\mathrm{Re}(A_m)\frac{\partial \mathrm{Re}(A_m)}{\partial \boldsymbol{p}_w} + \mathrm{Im}(A_m)\frac{\partial \mathrm{Im}(A_m)}{\partial \boldsymbol{p}_w}\right\} \quad \text{for} \quad m = 0 \tag{26}$$

$$\frac{\partial G_{pp,m}}{\partial \boldsymbol{p}_w} = 4\frac{T}{N^2}\left\{\mathrm{Re}(A_m)\frac{\partial \mathrm{Re}(A_m)}{\partial \boldsymbol{p}_w} + \mathrm{Im}(A_m)\frac{\partial \mathrm{Im}(A_m)}{\partial \boldsymbol{p}_w}\right\} \quad \text{for} \quad 1 \leq m \leq \frac{N}{2} - 1 \tag{27}$$

The sensitivities of the Fourier coefficients are shown in Eq. 28.

$$\frac{\partial \mathrm{Re}(A_m)}{\partial p_{w,n}} = \cos\left(\frac{2\pi nm}{N}\right), \qquad \frac{\partial \mathrm{Im}(A_m)}{\partial p_{w,n}} = -\sin\left(\frac{2\pi nm}{N}\right) \tag{28}$$

Then, combining Eq. 28 with Eq. 26 through Eq. 27, the sensitivity of the PSD with respect to the windowed APTH is then

$$\frac{\partial G_{pp,m}}{\partial p_{w,n}} = 2\frac{T}{N^2}\left\{\mathrm{Re}(A_m)\cos\left(\frac{2\pi nm}{N}\right) - \mathrm{Im}(A_m)\sin\left(\frac{2\pi nm}{N}\right)\right\} \quad \text{for} \quad m = 0 \tag{29}$$

$$\frac{\partial G_{pp,m}}{\partial p_{w,n}} = 4\frac{T}{N^2}\left\{\mathrm{Re}(A_m)\cos\left(\frac{2\pi nm}{N}\right) - \mathrm{Im}(A_m)\sin\left(\frac{2\pi nm}{N}\right)\right\} \quad \text{for} \quad 1 \leq m \leq \frac{N}{2} - 1 \tag{30}$$

It is important to comment on the technique employed to complex differentiate the Fourier transform. The input into the Fourier transform in the noncomplex differentiated algorithm is an array of purely real numbers that represent the acoustic pressure time history, $p_{w,n}$. The challenge lies in complex differentiating the already complex Fourier coefficients, A_m, while retaining the computational efficiency of the fast Fourier transform. Instead of following an approach similar to Reference 15, the authors found a different approach that provided very accurate results with significantly fewer code modifications. The complex differentiated acoustic pressure time history is defined as $\widetilde{p_{w,n}} = p_{w,n} + i\widehat{p_{w,n}}$, where the hat represents the complex component and the tilde represents the complex differentiated acoustic pressure time history. Then, by taking advantage of the definition of the Fourier transform, the complex differentiated Fourier coefficients can be defined as the following

$$\widetilde{\mathrm{Re}(A_m)} = \mathrm{Re}(A_m) + i\mathrm{Re}(\widehat{A_m}), \qquad \widetilde{\mathrm{Im}(A_m)} = \mathrm{Im}(A_m) + i\mathrm{Im}(\widehat{A_m}) \tag{31}$$

Taking advantage of Eq. 31, only the addition of one call to a fast Fourier transform package provides all that is required to complex differentiate the Fourier transform operation.

Figure 5 shows the sensitivity of PSD with respect to a representative windowed APTH using the FD, CD, and ND approaches. The representative windowed APTH consisted of a Hanning window applied to a time history of 40 periods of a 209.4 Hz sine wave. The amplitude of the sine wave was 1.148 Pa. The

perturbation values for the CD and FD approaches were ϵ of 10^{-10} Pa and Δ of 1% of the amplitude of the sine wave, respectively. The binwidth of the PSD was approximately 6 Hz and the sensitivity of the PSD was the only nonzero in the adjacent bins of the peak frequency. Relative error between the ND and FD approaches was 1.369×10^{-10}% and between the ND and CD approaches was 5.726×10^{-15}%. As expected, the relative error between the ND and CD approaches was lower due to the inherent numerical inaccuracies in the FD approach.

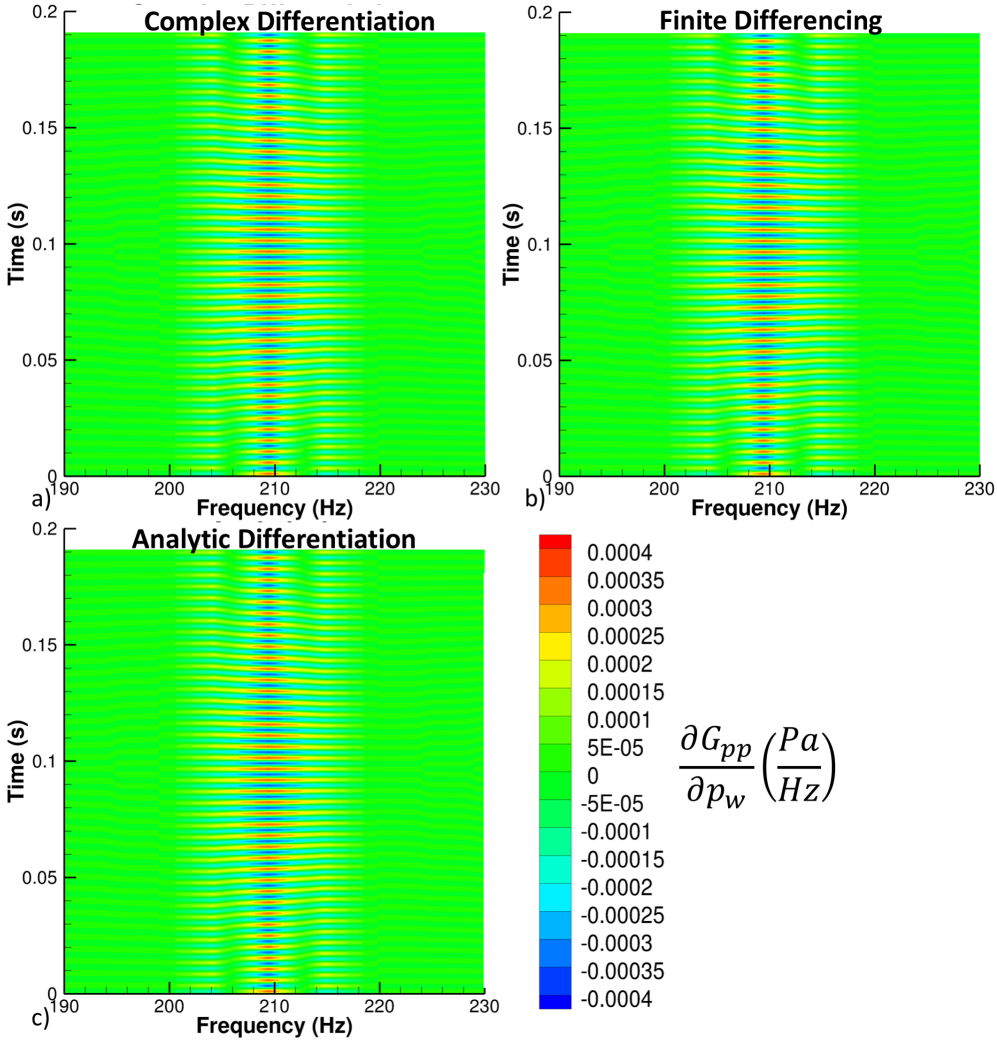

Figure 5. Sensitivity of PSD with respect to windowed APTH using a) CD, b) FD, and c) ND.

E. Proportional Band Sound Pressure Level Spectrum

A proportional band SPL spectrum (PBS), such as a 1/3-octave band SPL spectrum, quantifies the acoustic energy within a band of frequencies defined by an upper and lower limit, f_u and f_l. The energy is determined by integrating the PSD to achieve a mean square pressure per band, denoted by $\langle p^2 \rangle_b$. The SPL is then

determined as a log function relative to a reference pressure, p_{ref}, typically 2×10^{-5} Pa. This is shown in Eq. 32. The analytic sensitivity can be found via the chain rule, shown in Eq. 33.

$$\langle p^2 \rangle_b = \int_{f_{l,b}}^{f_{u,b}} G_{pp} df, \qquad \mathrm{L}_{\mathrm{B},b} = 10 \log_{10} \frac{\langle p^2 \rangle_b}{p_{\text{ref}}^2} \tag{32}$$

$$\frac{\partial \mathrm{L}_{\mathrm{B},b}}{\partial G_{pp,m}} = \frac{10}{\ln 10} \frac{G_{pp,m} \Delta f_m}{\langle p^2 \rangle_b} \qquad \text{when} \qquad f_{l,b} \leq f_m \leq f_{u,b} \tag{33}$$

Validation of the sensitivity calculated using the ND approach was performed using a representative PSD spectrum shown in Fig. 6. The perturbation values for the CD and FD approaches were ϵ of 10^{-10} $\mathrm{Pa}^2/\mathrm{Hz}$ and Δ of 1% of the maximum value of the PSD, respectively. The sensitivities using the ND, CD, and FD approaches are shown in Fig. 7. The relative total error between the ND approach and the FD approach was 2.174×10^{-10}%; and between the ND and CD approaches was 2.502×10^{-15}%. As expected, the sensitivities using the ND approach were closer to those found using the CD approach.

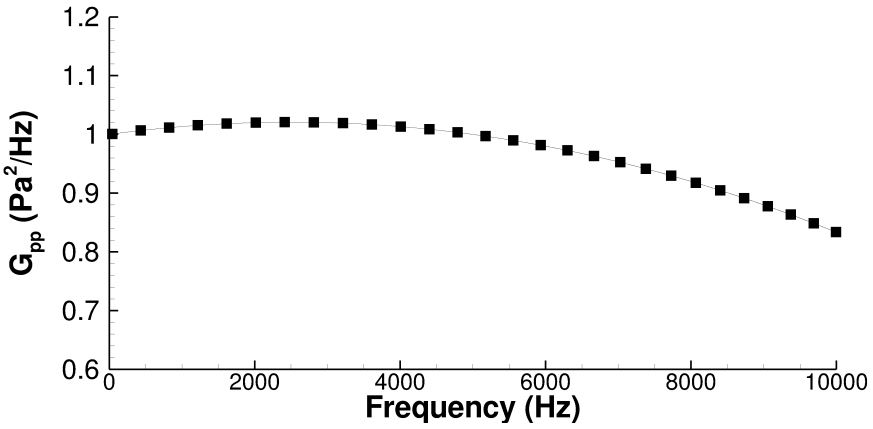

Figure 6. Representative windowed PSD used as input in the validation of the sensitivity of proportional band SPL spectrum.

F. Frequency Weighting

Weighting functions are used to numerically alter recorded sound to more accurately represent a human's response to noise. While the PSD is a measure of the physical properties of an acoustic signal, it does not accurately reflect what people hear. This is because the sensitivity of the human auditory system is strongly dependent on the intensity and frequency of the sound. Frequency weighting methods were developed to simulate the change in annoyance of measured sound due to the human ear and psychological factors, i.e., attenuating low frequencies and very high frequencies, while leaving midfrequencies almost unchanged[16,17]. There are several different frequency weighting algorithms commonly used in acoustics, including A-, B-, C-, and D-weighting algorithms. Regardless of the frequency weighting algorithm, the weighting operation is a

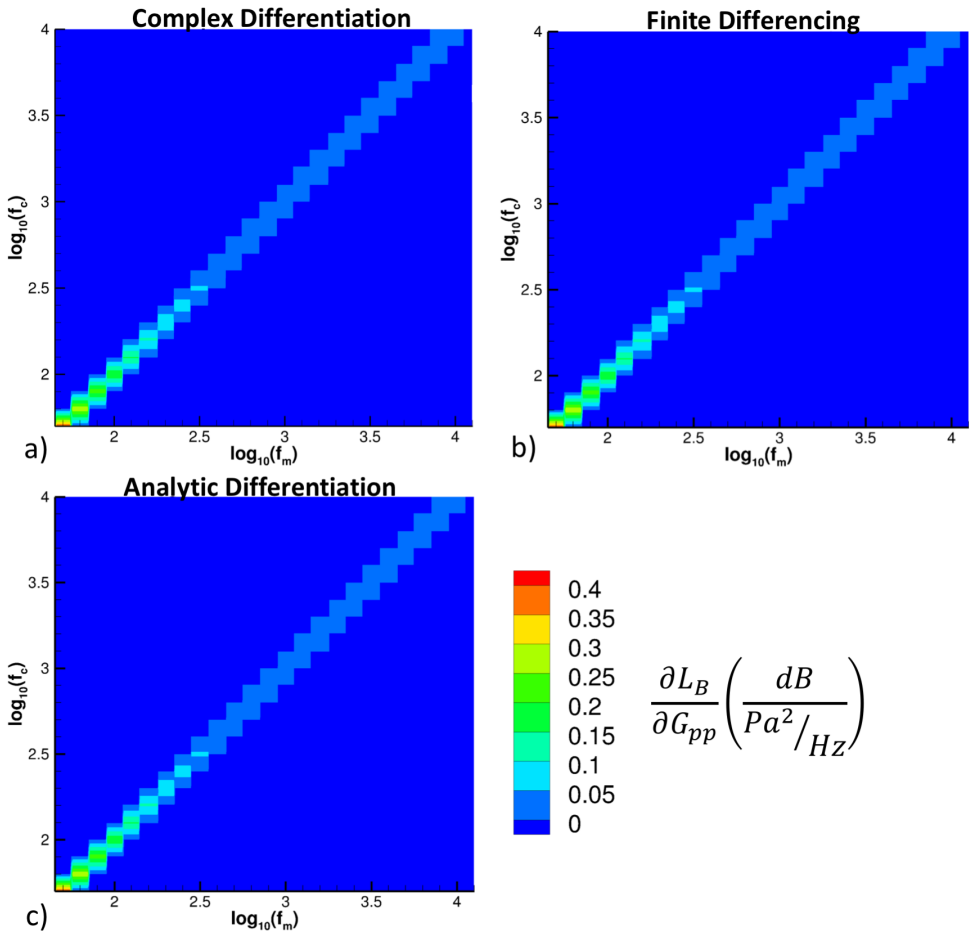

Figure 7. Sensitivity of PBS with respect to representative windowed PSD using the a) CD, b) FD, and c) ND.

simple multiplication at each bin frequency, shown in Eq. 34, where W is the weighting function (i.e., A-, B-, C-, or D-weighting), m and m' are each bin in the PSD, and f_m is the frequency at the mth bin. Also shown in Eq. 34 is the sensitivity of this operation where δ is the Dirac delta function. Frequency weighting can also be applied directly to the 1/3-octave band SPL spectrum. This is shown, with sensitivity, in Eq. 35, where $f_{c,b}$ is the center band frequency of band b.

$$G_{pp,W,m} = G_{pp,m} W(f_m), \qquad \frac{\partial G_{pp,W,m}}{\partial G_{pp,m'}} = \delta_{mm'} W(f_m) \tag{34}$$

$$\mathrm{L}_{\mathrm{B},W,b} = \mathrm{L}_{\mathrm{B},b} + 10\log_{10}(W(f_{c,b})), \qquad \frac{\partial \mathrm{L}_{\mathrm{B},W,b}}{\partial \mathrm{L}_{\mathrm{B},b'}} = \delta_{b,b'} \tag{35}$$

Figure 8 shows a comparison between the sensitivities calculated by the CD, FD, and the ND approaches shown in Eq. 34 with an A-weighting function. The PSD used as input to the validation was composed of a constant value of 1 $\mathrm{Pa}^2/\mathrm{Hz}$ across a frequency range of 50 Hz to 10 kHz. The perturbation values for the CD

and FD approaches were ϵ of 10^{-10} Pa^2/Hz and Δ of 1% of the amplitude of the mean-square pressure (MSP) value at the perturbation frequency, respectively. The total percent error between sensitivities calculated using the ND and FD approaches was 8.709×10^{-14}% and between the sensitivities calculated using the ND and CD approaches was 1.734×10^{-15}%. As expected, the sensitivities calculated using the ND and CD approaches were much closer than those calculated using the FD and ND approaches due to numerical inaccuracies in the finite differencing.

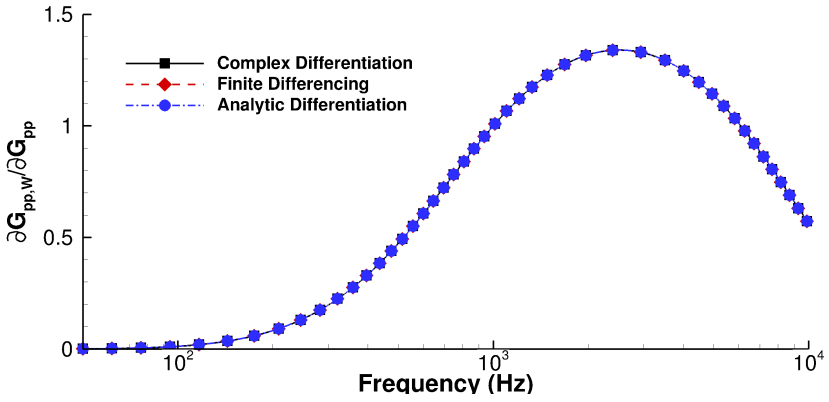

Figure 8. Sensitivity of A-weighting algorithm using the CD, FD, and ND approaches.

G. Overall Sound Pressure Level

The A-weighted OASPL is defined by Eq. 36, where $\langle p^2 \rangle_{\mathrm{L_A}}$ is the A-weighted total mean square acoustic pressure and p_{ref} is a reference pressure, typically 2×10^{-5} Pa. The total mean square acoustic pressure is defined as the total acoustic energy within a range of frequencies, usually the total range (thus 'overall'). Equation 37 shows the calculation of the total mean square acoustic pressure from a PSD and from a 1/3-octave band SPL spectrum where M is the total number of bins in the PSD and B is the total number of bands in the 1/3-octave band SPL spectrum. Equation 38 shows the sensitivity of the A-weighted OASPL from either the PSD or 1/3-octave band SPL spectrum. It is important to note that although A-weighted OASPL is being shown here, similar analysis can be used to any other weighting function, including no weighting.

$$\mathrm{L_A} = 10\log_{10}\left\{\frac{\langle p^2 \rangle_{\mathrm{L_A}}}{p_{\mathrm{ref}}^2}\right\} \tag{36}$$

$$\langle p^2 \rangle_{\mathrm{L_A}} = \Delta f \sum_{m=1}^{M} G_{pp,\mathrm{A},m}, \qquad \langle p^2 \rangle_{\mathrm{L_A}} = p_{\mathrm{ref}}^2 \sum_{b=1}^{B} 10^{\mathrm{L_{B,A},}b/10} \tag{37}$$

$$\frac{\partial \mathrm{L_A}}{\partial G_{pp,\mathrm{A},m}} = \frac{10}{\ln(10)} \frac{1}{\langle p^2 \rangle_{\mathrm{L_A}}} \Delta f, \qquad \frac{\partial \mathrm{L_A}}{\partial \mathrm{L_{B,A},}b} = \frac{\langle p^2 \rangle_{A,b}}{\langle p^2 \rangle_{\mathrm{L_{B,A}}}} \tag{38}$$

Figure 9a) shows a representative PSD with 1 Hz binwidth and Fig. 9b) shows the sensitivity calculated via the CD, FD, and ND approaches. The perturbation values for the CD and FD approaches was an ϵ of 10^{-10} Pa^2/Hz and Δ of 0.01 times the PSD mean square pressure, respectively. The total relative error between the ND and FD approaches was $1.580 \times 10^{-7}\%$ and between the ND and CD approaches was $2.390 \times 10^{-14}\%$. The relative error between the ND and FD approaches was much higher than between the ND and CD approaches due to inaccuracies in the finite differencing.

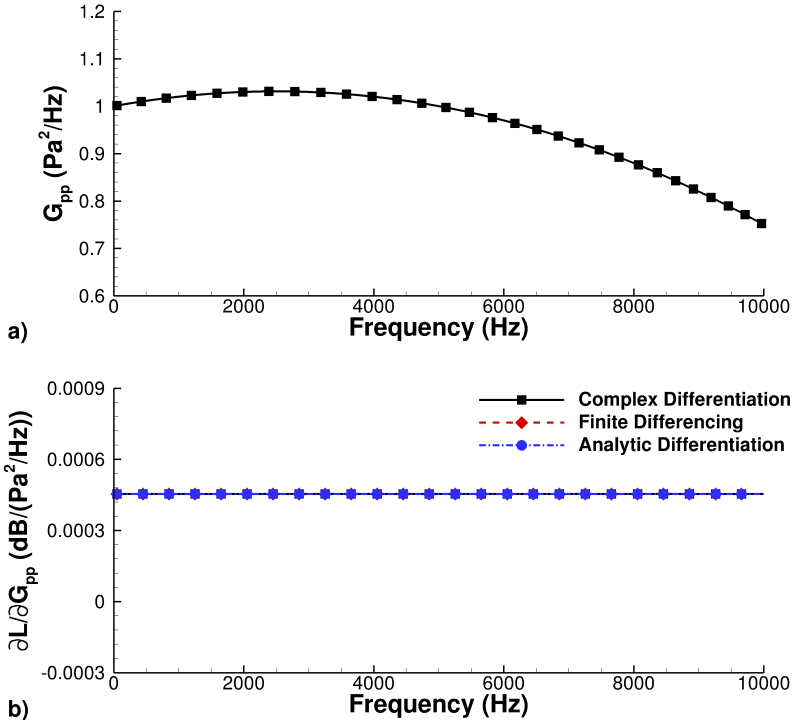

Figure 9. a) Representative PSD. b) Sensitivity of OASPL with respect to PSD using the CD, FD, and ND approaches.

H. Tone-Corrected Perceived Noise Level

The process for calculating a PNLT is outlined in the Code of Federal Regulations (CFR) Title 14 Part 36[18] and involves several steps including calculating a Perceived Noise Level (PNL) then adjusting it for any tones in the 1/3-octave band SPL spectrum. The equation for PNLT, including sensitivity, is shown in Eq. 39. For brevity, the algorithm for calculating PNLT and its sensitivity are shown in Appendix A.

$$\text{PNLT} = \text{PNL} + C_{\max}, \qquad \frac{\partial \text{PNLT}}{\partial \mathbf{L}_\text{B}} = \frac{\partial \text{PNL}}{\partial \mathbf{L}_\text{B}} + \frac{\partial C_{\max}}{\partial \mathbf{L}_\text{B}} \tag{39}$$

Figure 10a) shows a representative 1/3-octave band SPL spectrum, Fig. 10b) shows the sensitivity of the PNL, and Fig. 10c) shows the sensitivity of the PNLT. The perturbation values for the CD and FD

approaches were ϵ of 10^{-10} dB and Δ of 0.01 dB, respectively. The total relative error between the ND and FD approaches was $3.600 \times 10^{-7}\%$ and between the ND and CD approaches was $7.202 \times 10^{-16}\%$. The relative error between the ND and FD approaches was much higher than between the ND and CD approaches due to inaccuracies in the finite differencing. Comparing Fig. 10b) and 10c) highlights the importance of the tone correction to the PNLT values. The peak in Fig. 10b) and 10c) at 3kHz is due to the noisiness table; a shift in the SPL value at this center band frequency moves the value of noisiness in this band to a larger value, thus the high sensitivity. It is interesting to note that, for this representative case, an increase in noise in the 100 or 160 Hz band results in a reduction of PNLT due to the tone correction.

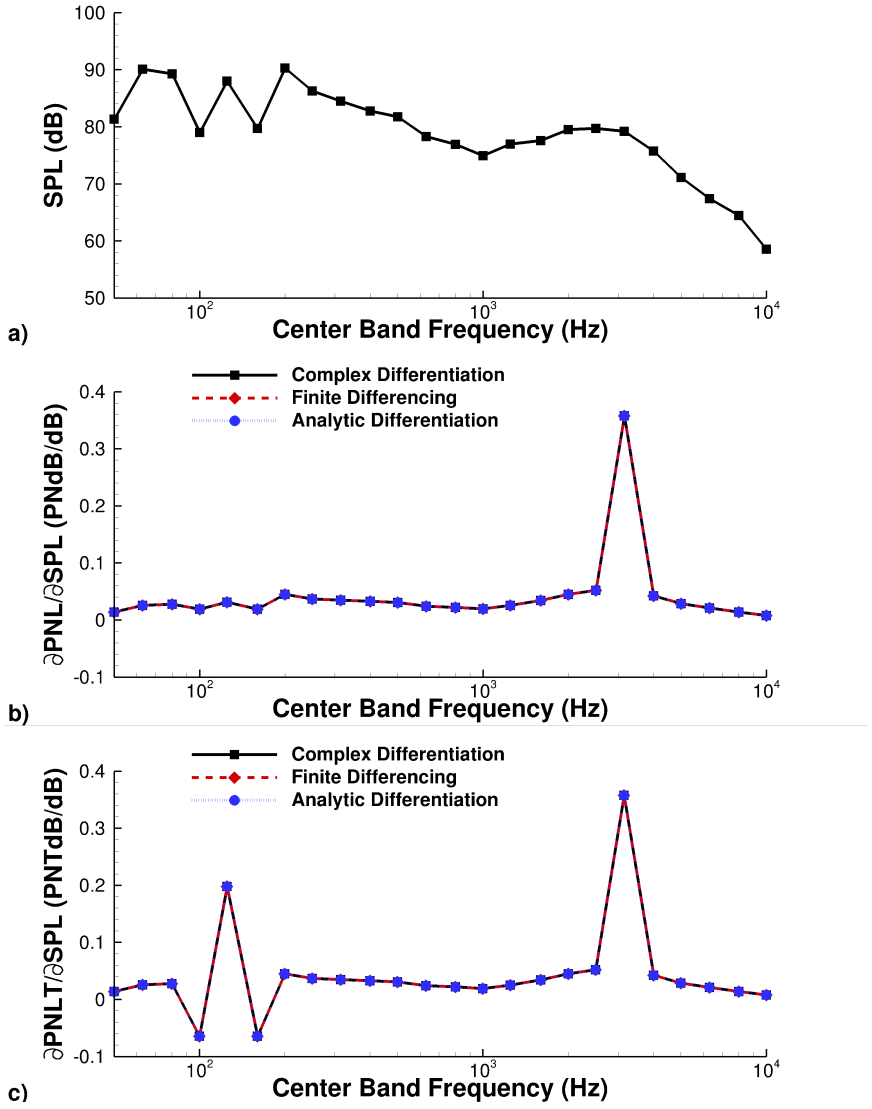

Figure 10. a) Representative 1/3-octave band SPL spectrum. b) Sensitivity of PNL with respect to SPL using CD, FD, and ND. c) Sensitivity of the PNLT with respect to SPL using CD, FD, and ND.

I. Effective Perceived Noise Level

The EPNL is determined through an integration of the PNLT over a time range when the PNLT is greater than the maximum PNLT minus 10 decibels, defined by the interval of t_i to t_f, and normalization constant T of 10 seconds. This is shown in Eq. 40.

$$\mathrm{EPNL} = 10 \log_{10} \frac{1}{T} \int_{t_i}^{t_f} 10^{\mathrm{PNLT}/10} dt \tag{40}$$

The change in the limits of the integration due to the maximum EPNL value does not have to be included in the analytic formulation for sensitivity because of the algorithm defined in the Code of Federal Regulations (CFR) Title 14 Part 36[18]. These ranges do not change with a small change in PNLT because the EPNL algorithm picks the closest known value. The sensitivity is determined by Eq. 41.

$$\frac{\partial \mathrm{EPNL}}{\partial \mathrm{PNLT}_j} = \left\{ \int_{t_i}^{t_f} 10^{\mathrm{PNLT}/10} dt \right\}^{-1} 10^{\mathrm{PNLT}_j/10} \Delta t \tag{41}$$

Figure 11a) shows a representative PNLT time history and Fig. 11b) shows the sensitivity calculated through Eq. 41, as well as from the CD and FD approaches using a perturbation value of ϵ of 10^{-10} PNdB and Δ of 0.01 PNdB, respectively. The total relative error between the ND and FD approaches was $2.268 \times 10^{-7}\%$ and between the ND and CD approaches was $5.417 \times 10^{-16}\%$. The relative error between the ND and FD approaches was much higher than that between the ND and CD approaches due to numerical inaccuracies in the finite differencing.

J. Sound Exposure Level

The definition of Sound Exposure Level (SEL), shown in Eq. 42, includes an integration of A-weighted OASPL over a range t_i to t_f and includes a normalization constant T of 1 second. The time range, in practice, is defined as the time when A-weighted OASPL is above 10dB down from the peak level, $\mathrm{L}_{\mathrm{A},M}$.

$$\mathrm{SEL} = 10 \log_{10} \frac{1}{T} \int_{t_i}^{t_f} 10^{\mathrm{L_A}/10} dt \tag{42}$$

Unlike EPNL, SEL requires a redefinition of the limits of integration due to the change in the maximum value. By simple mathematical operations and taking advantage of the Leibniz rule for differentiation under the integral sign, the sensitivity of SEL with respect to A-weighted OASPL is

$$\frac{\partial \mathrm{SEL}}{\partial \mathrm{L}_{\mathrm{A},j}} = \left\{ \frac{10}{\ln 10} \right\} \left\{ \int_{t_i}^{t_f} 10^{\mathrm{L_A}/10} dt \right\}^{-1} \left[\left\{ \frac{\ln 10}{10} \right\} 10^{\mathrm{L}_{\mathrm{A},j}/10} \Delta t + 10^{(\mathrm{L}_{\mathrm{A},M}-10)/10} \left(\frac{\partial t_f}{\partial \mathrm{L}_{\mathrm{A},j}} - \frac{\partial t_i}{\partial \mathrm{L}_{\mathrm{A},j}} \right) \right] \tag{43}$$

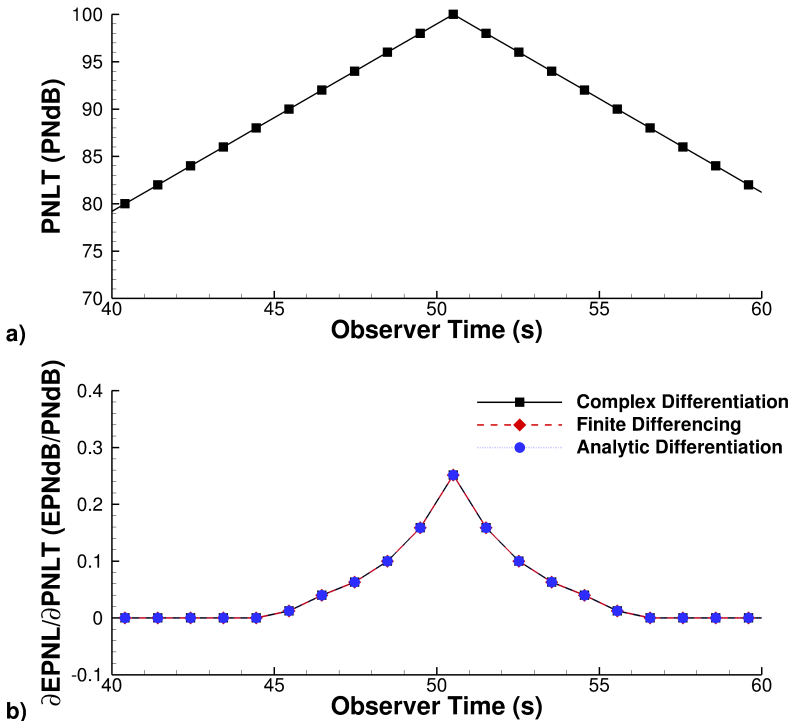

Figure 11. a) Representative PNLT time history. b) Sensitivity of EPNL with respect to PNLT using CD, FD, and ND.

Figure 12a) shows a representative A-weighted OASPL time history and Fig. 12b) shows the sensitivity calculated through Eq. 43 as well as the CD and FD approaches using an ϵ of 10^{-10} dBA and Δ of 0.01 dBA, respectively. The total relative error between the ND and FD approaches was $9.641 \times 10^{-3}\%$ and between the ND and CD approaches was $1.209 \times 10^{-14}\%$. The relative error between the ND and FD approaches was much higher than between the ND and CD approaches due to inaccuracies in the finite differencing.

K. Single Event Noise Exposure Level

The Single Event Noise Exposure Level (SENEL) is a metric similar to SEL in that it is a noise level, measured in dB, of a single event, such as an aircraft flyby, measured over a time interval between the initial and final times for which the noise level of a single event exceeds a predetermined threshold noise level[19]. Since the predetermined threshold, and thus the limits of integration, are defined by the configuration, the sensitivity of SENEL behaves like the sensitivity of EPNL, in that the change in integration limits are no longer a function of the levels, but must be taken into account by the calling functionality. The definition of SENEL is shown in Eq. 44, and the sensitivity of SENEL is shown in Eq. 45. Validation of the sensitivity of

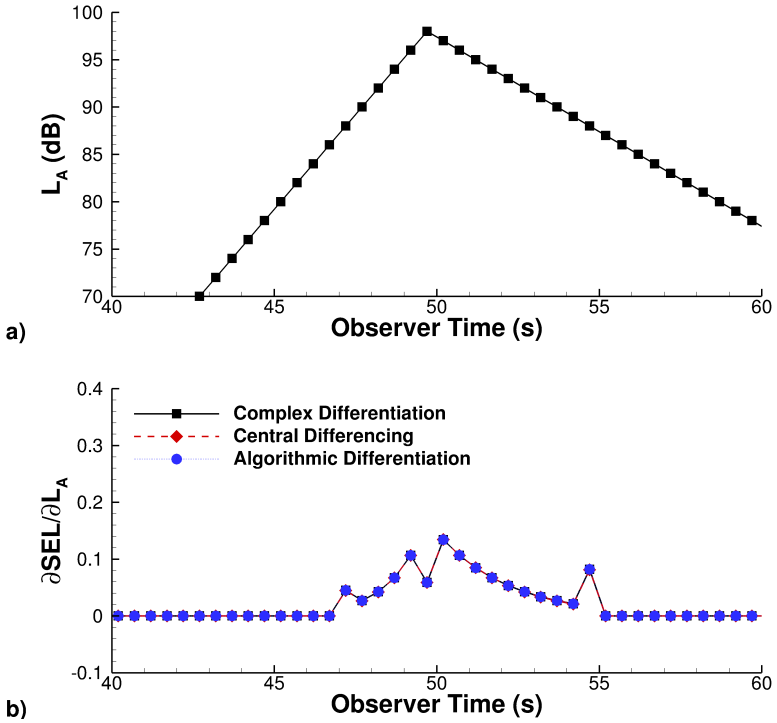

Figure 12. a) Representative OASPL time history. b) Sensitivity of SEL with respect to OASPL using CD, FD, and ND.

SENEL is very similar to validation of the sensitivity of EPNL and SEL, and is left out for brevity.

$$\mathrm{SENEL} = 10 \log_{10} \frac{1}{T} \int_{t_i}^{t_f} 10^{\mathrm{L_A}/10} dt \tag{44}$$

$$\frac{\partial \mathrm{SENEL}}{\partial \mathrm{L_{A,}}_j} = \left\{ \int_{t_i}^{t_f} 10^{\mathrm{L_A}/10} dt \right\}^{-1} 10^{\mathrm{L_A}_j/10} \Delta t \tag{45}$$

L. Exposure Area

The exposure area is a measure of the ground surface area affected by a noise level, such as EPNL or SEL, greater than or equal to a specified limit, $\mathscr{L}$. Currently, ANOPP2 can calculate the exposure area given the noise levels on a structured or unstructured mesh, defined as a set of levels, L_i, and coordinates, $[x, y]_i$, where subscript i denotes node value. Using linear interpolation, a polygon is defined for each cell within the structured mesh where the noise levels are above the specified limit. The total exposure area is then the sum of all polygon areas; this is shown in Eq. 46 where N is the total number of polygons, A_n is the area from the n^{th} polygon, $[x, y]_{n,m}$ is the m^{th} polygon vertex expressed in Cartesian coordinates, and M is the number of sides of the polygon (3, 4, 5, or 6). To form a closed polygon, the $M + 1$ vertex coincides with the first vertex of the polygon. Equation 47 shows the linear interpolation of vertex $[x, y]_n$ that falls

between nodes $[x,y]_i$ and $[x,y]_{i+1}$. Fig. 13a) shows an example exposure area calculation using ANOPP2; in the example, levels fall off as a function of one over the radius, and the specified limit is defined such that the area approaches π as the mesh resolution increases.

$$\mathrm{EA} = \sum_{n=1}^{N} A_n, \qquad A_n = \frac{1}{2}\sum_{m=1}^{M}(x_{n,m}y_{n,m+1} - x_{n,m+1}y_{n,m}) \tag{46}$$

$$[x,y]_m = [x,y]_i + \frac{\mathscr{L} - L_i}{L_{i+1} - L_i}([x,y]_{i+1} - [x,y]_i) \tag{47}$$

Figs. 13b) through d) show the sensitivities calculated through the ND approach via Eqs. 48 through 50,[d] as well as the CD and FD approaches. Sensitivities calculated using the CD and FD approaches used an ϵ of 10^{-10} dB and Δ of 0.01 dB, respectively. The total relative error between ND and FD is $8.243 \times 10^{-8}\%$ and between ND and CD is $3.225 \times 10^{-14}\%$. The relative error between the ND and FD approaches is much higher than between the ND and CD approaches due to inaccuracies in the finite differencing.

$$\frac{\partial \mathrm{EA}}{\partial L_i} = \frac{\partial \mathrm{EA}}{\partial \boldsymbol{A}}\frac{\partial \boldsymbol{A}}{\partial L_i}, \qquad \frac{\partial \mathrm{EA}}{\partial A_n} = 1 \tag{48}$$

$$\frac{\partial A_n}{\partial L_i} = \frac{1}{2}\sum_{m=1}^{M}\left\{\frac{\partial x_{n,m}}{\partial L_i}y_{n,m+1} + x_{n,m}\frac{\partial y_{n,m+1}}{\partial L_i} - \frac{\partial x_{n,m+1}}{\partial L_i}y_{n,m} - x_{n,m+1}\frac{\partial y_{n,m}}{\partial L_i}\right\} \tag{49}$$

$$\frac{\partial [x,y]_m}{\partial L_i} = \frac{\mathscr{L} - L_{i+1}}{(L_{i+1} - L_i)^2}([x,y]_{i+1} - [x,y]_i), \qquad \frac{\partial [x,y]_m}{\partial L_{i+1}} = \frac{L_i - \mathscr{L}}{(L_{i+1} - L_i)^2}([x,y]_{i+1} - [x,y]_i) \tag{50}$$

IV. Acoustic Objective Function Demonstration Case

A simple demonstration case was constructed that showcases the usage of acoustic metric sensitivities in the minimization of a noise metric. In the demonstration, a point monopole was placed above a grid of observers, a schematic of which is shown in Fig. 14. The strength of the point monopole, S, was defined according to a quadratic function of the height above the observer grid, shown in Eq. 51, where H is the height above the observer grid. This function was constructed arbitrarily purely to demonstrate the usage of the sensitivities. A square grid of 11 by 11 observer nodes was constructed and sized 50 m by 50 m. The acoustic pressure was determined using Eq. 52, where x_i and y_i are the observer coordinates on the ground of the ith observer, $\vec{r_i}$ is the radiation vector of length r_i, f is the frequency of the source (10 Hz), c is the speed of sound (343 m/s), t_n is the nth observer time ranging from 0 to 1 with 101 time steps, j is $\sqrt{-1}$, and $p_{n,i}$ is the acoustic pressure at the ith observer at time step n. An OASPL, L, was then calculated at

[d] Eqs. 48 through 50 assume a counter-clockwise definition of the polygon vertices.

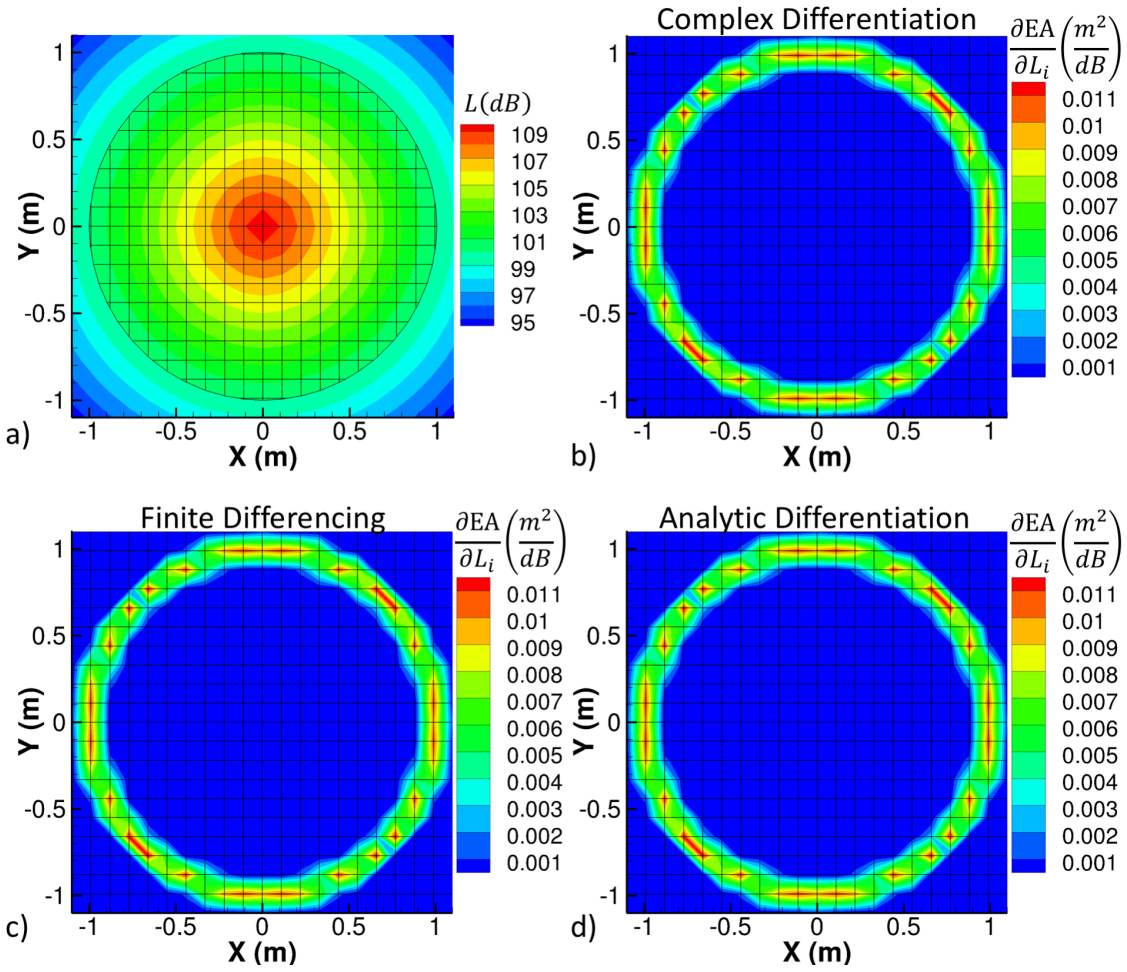

Figure 13. a) Representative exposure area calculation showing all polygons. Also shown is $\frac{\partial \mathrm{EA}}{\partial L_i}$ calculated via b) CD, c) FD, and d) ND.

each observer point from the acoustic pressure time series by first calculating a PSD, G_{pp}. After the OASPL was calculated at all the observer nodes, an exposure area, EA, with an 80 dB limit was calculated.

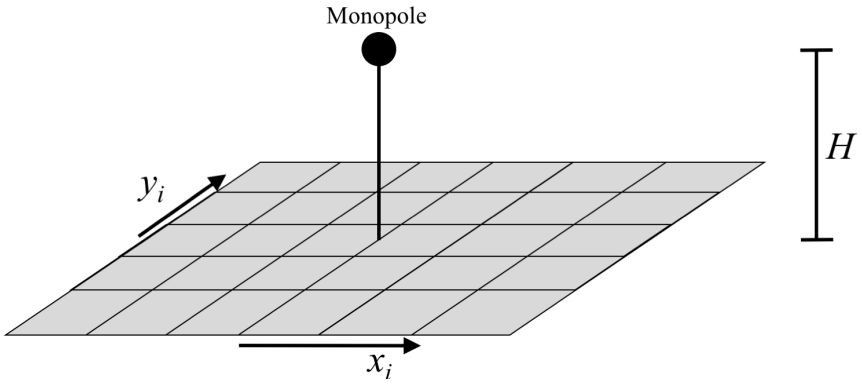

Figure 14. Schematic of exposure area optimization demonstration case.

$$S = 10 - 0.1250H + 0.01250H^2 \tag{51}$$

$$p_{n,i} = \frac{S}{r_i} e^{2\pi f j (t_n - \frac{r_i}{c})}, \qquad r_i = |\vec{r}_i| = \sqrt{x_i^2 + y_i^2 + H^2} \tag{52}$$

The sensitivity of the target acoustic metric, exposure area, with respect to height, shown in Eq. 53, was defined by the symbolic differentiation of the equation for the acoustic pressure, shown in Eq. 54, and the analytic differentiation of PSD and OASPL, shown in the previous sections.

$$\frac{\partial \mathrm{EA}}{\partial H} = \left\{ \frac{\partial \mathrm{EA}}{\partial \boldsymbol{p}} \right\} \frac{\partial \boldsymbol{p}}{\partial H} = \left\{ \frac{\partial \mathrm{EA}}{\partial \mathbf{L}} \frac{\partial \mathbf{L}}{\partial \boldsymbol{G}_{pp}} \frac{\partial \boldsymbol{G}_{pp}}{\partial \boldsymbol{p}} \right\} \frac{\partial \boldsymbol{p}}{\partial H} \tag{53}$$

$$\frac{\partial p_{n,i}}{\partial H} = \left[\frac{1}{r_i} \frac{\partial S}{\partial H} - \frac{SH}{r_i^2} \left\{ \frac{1}{r_i} + \frac{2\pi f j}{c} \right\} \right] e^{2\pi f j (t_n - \frac{r_i}{c})} \tag{54}$$

The height associated with the minimum of the source strength function, 5.000 m, was used as a first guess at a minimum exposure area. Using the sensitivities of the exposure area with respect to height and the method of steepest decent, shown in Eq. 55, a minimum exposure area within 0.1 m^2 was found with 5 iterations. The height, source strength, exposure area, and exposure area sensitivity with respect to height are shown in Table 1.

$$H_n = H_{n-1} - 0.1 \frac{\partial \mathrm{EA}}{\partial H} \tag{55}$$

Table 1. Iteration, height, source strength, exposure area, and exposure area sensitivity with respect to height for each iteration of the demonstration case.

Iteration	Height (m)	Source Strength (N/m)	Exposure Area (m^2)	$\partial EA/\partial H$ (m)
1	5.000	9.6875	3588.5	-32.76
2	8.249	9.8195	3551.0	10.32
3	7.217	9.7490	3548.0	-3.591
4	7.576	9.7705	3547.4	1.213
5	7.455	9.7628	3547.4	-0.4142

V. Conclusion

This paper presented an approach to include robust acoustic objective functions in design optimizations. It was shown that including acoustics in adjoint, CFD-based design optimizations requires the sensitivity of the acoustic objective function, which can be represented by any number of acoustic metrics within ANOPP2. The analytic sensitivity of several acoustic metrics available in ANOPP2 were derived and validated by comparing to those obtained using complex differentiation and finite differencing. A demonstration was performed that calculated the minimal exposure area from a monopole whose strength was a function of height above a grid of observers.

A. Algorithm for the Sensitivity of Tone-Corrected Perceived Noise Level

The algorithm for calculating the sensitivity of PNLT involves several steps. Taking the first term in Eq. 56, the sensitivity of the PNL with respect to the 1/3-octave band SPL spectrum is defined via the chain rule, shown in Eq. 56.

$$\frac{\partial \mathrm{PNL}}{\partial \mathbf{L}_B} = \frac{\partial \mathrm{PNL}}{\partial N_t} \frac{\partial N_t}{\partial \boldsymbol{N}} \frac{\partial \boldsymbol{N}}{\partial \mathbf{L}_B} \tag{56}$$

The PNL is a function of the total perceived noisiness, N_t, which is in turn a function of the noisiness of each band, $\boldsymbol{N}$. The definition of PNL, including its sensitivity to the total perceived noisiness, is shown in Eq. 57. The total perceived noisiness, including its sensitivity to the noisiness is shown in Eq. 58.

$$\mathrm{PNL} = 40 + \frac{10}{\log_{10} 2} \log_{10}(N_t) \qquad \frac{\partial \mathrm{PNL}}{\partial N_t} = \frac{10}{\log_{10} 2} \frac{1}{\ln(10) N_t} \tag{57}$$

$$N_t = 0.85 N_{max} + 0.15 \sum_{b=1}^{24} N_b \qquad \frac{\partial N_t}{\partial N_b} = \begin{cases} 0.15 & N_b \neq N_{\max} \\ 1.0 & N_b = N_{\max} \end{cases} \tag{58}$$

The final part of the sensitivity of the PNL with respect to the 1/3-octave band SPL spectrum is the

sensitivity of the noisiness to the 24 1/3-octave band SPLs. The definition of the noisiness is shown in Eq. 59 and its sensitivity is shown in Eq. 60. Constants used in Eq. 59 and 60 are shown in Table 2.

$$N_b = \begin{cases} 10^{M(c)[\mathrm{L_{B},}_b - \mathrm{SPL}(c)]} & \mathrm{L_{B},}_b \geq \mathrm{SPL}(a) \\ 10^{M(b)[\mathrm{L_{B},}_b - \mathrm{SPL}(b)]} & \mathrm{SPL}(b) \leq \mathrm{L_{B},}_b < \mathrm{SPL}(a) \\ 0.3 \times 10^{M(e)[\mathrm{L_{B},}_b - \mathrm{SPL}(e)]} & \mathrm{SPL}(e) \leq \mathrm{L_{B},}_b < \mathrm{SPL}(b) \\ 0.1 \times 10^{M(d)[\mathrm{L_{B},}_b - \mathrm{SPL}(d)]} & \mathrm{SPL}(d) \leq \mathrm{L_{B},}_b < \mathrm{SPL}(e) \end{cases} \tag{59}$$

$$\frac{\partial N_{b'}}{\partial \mathrm{L}_{B,b}} = \begin{cases} (\ln 10) M(c) 10^{M(c)[\mathrm{L_{B},}_b - \mathrm{SPL}(c)]} & b' = b \;\; \& \;\; \mathrm{L_{B},}_b \geq \mathrm{SPL}(a) \\ (\ln 10) M(b) 10^{M(b)[\mathrm{L_{B},}_b - \mathrm{SPL}(b)]} & b' = b \;\; \& \;\; \mathrm{SPL}(b) \leq \mathrm{L_{B},}_b < \mathrm{SPL}(a) \\ 0.3(\ln 10) M(e) 10^{M(e)[\mathrm{L_{B},}_b - \mathrm{SPL}(e)]} & b' = b \;\; \& \;\; \mathrm{SPL}(e) \leq \mathrm{L_{B},}_b < \mathrm{SPL}(b) \\ 0.1(\ln 10) M(d) 10^{M(d)[\mathrm{L_{B},}_b - \mathrm{SPL}(d)]} & b' = b \;\; \& \;\; \mathrm{SPL}(d) \leq \mathrm{L_{B},}_b < \mathrm{SPL}(e) \\ 0 & b' \neq b \end{cases} \tag{60}$$

To calculate the tone correction is a process involving several additional steps that can be broken down into three components via the chain rule, shown in Eq. 61, where $\boldsymbol{C}$ is a tone-correction factor at each band, and $\boldsymbol{F}$ is called a 'difference' in the Code of Federal Regulations (CFR) Title 14 Part 36 at each band[18].

$$\frac{\partial C_{\max}}{\partial \mathbf{L}_{\mathrm{B}}} = \frac{\partial C_{\max}}{\partial \boldsymbol{C}} \frac{\partial \boldsymbol{C}}{\partial \boldsymbol{F}} \frac{\partial \boldsymbol{F}}{\partial \mathbf{L}_{\mathrm{B}}} \tag{61}$$

The change in maximum tone correction with respect to tone correction at each index is found by selecting the change in tone correction at the appropriate index corresponding to the maximum tone correction. The tone correction factor for frequencies in the range $50 \leq f_b < 500$ is shown in Eq, 62, for frequencies in the range $500 \leq f_b \leq 5000$ is shown in Eq. 63, and for frequencies in the range $5000 < f_b \leq 10000$ is shown in Eq. 64.

$$C_b = \begin{cases} 0 & F_b < 1\frac{1}{2} \\ \frac{1}{3} F_b - \frac{1}{2} & 1\frac{1}{2} \leq F_b < 3 \\ \frac{1}{6} F_b & 3 \leq F_b < 20 \\ 3\frac{1}{3} & 20 \leq F_b \end{cases} \tag{62}$$

Table 2. Constants for calculation of noisiness values[18].

1/3-Octave Center Band Frequency Hz	SPL(a) dB	SPL(b) dB	SPL(c) dB	SPL(d) dB	SPL(e) dB	$M(b)$	$M(c)$	$M(d)$	$M(e)$
50	91.0	64	52	49	55	.043478	.030103	.079520	.058098
63	85.9	60	51	44	51	.040570	↑	.068160	.058098
80	87.3	56	49	39	46	.036831	↑	.068160	.052288
100	79.9	53	47	34	42	.036831	↑	.059640	.047534
125	79.8	51	46	30	39	.035336	↑	.053013	.043573
160	76.0	48	45	27	36	.033333	↑	↑	.043573
200	73.0	46	43	24	33	.033333	↑	↑	.040221
250	74.9	44	42	21	30	.032051	↑	↑	.037349
315	94.6	42	41	18	27	.030675	.030103	↑	.034859
400	∞	40	40	16	25	.030103		↑	↑
500	↑	40	40	16	25	↑		↑	↑
630	↑	40	40	16	25	↑		↑	↑
800	↑	40	40	16	25	↑	NOT	↑	↑
1000	↑	40	40	16	25	↑	APPLI	↑	↑
1250	↑	38	38	15	23	.030103	CABLE	.059640	.034859
1600	↑	34	34	12	21	.029960	↑	.053013	.040221
2000	↑	32	32	9	18	↑	↑	.053013	.037349
2500	↑	30	30	5	15	↑	↑	.047712	.034859
3150	↑	29	29	4	14	↑	↑	.047712	↑
4000	↑	29	29	5	14	↑	↑	.053013	↑
5000	↑	30	30	6	15	↑	↑	.053013	.034859
6300	∞	31	31	10	17	.029960		.068160	.037349
8000	44.3	37	34	17	23	.042285	.029960	.079520	.037349
10000	50.7	41	37	21	29	.042285	.029960	.059640	.043573

$$C_b = \begin{cases} 0 & F_b < 1\frac{1}{2} \\ \frac{2}{3}F_b - 1 & 1\frac{1}{2} \le F_b < 3 \\ \frac{1}{3}F_b & 3 \le F_b < 20 \\ 6\frac{2}{3} & 20 \le F_b \end{cases} \tag{63}$$

$$C_b = \begin{cases} 0 & F_b < 1\frac{1}{2} \\ \frac{1}{3}F_b - \frac{1}{2} & 1\frac{1}{2} \le F_b < 3 \\ \frac{1}{6}F_b & 3 \le F_b < 20 \\ 3\frac{1}{3} & 20 \le F_b \end{cases} \tag{64}$$

The sensitivity of the tone correction factor with respect to the difference for frequencies in the range $50 \le f_b < 500$ is shown in Eq, 65, for frequencies in the range $500 \le f_b \le 5000$ is shown in Eq. 66, and for frequencies in the range $5000 < f_b \le 10000$ is shown in Eq. 67.

$$\frac{\partial C_{b'}}{\partial F_b} = \begin{cases} 0 & b' = b \;\;\&\;\; F_b < 1\frac{1}{2} \\ \frac{1}{3} & b' = b \;\;\&\;\; 1\frac{1}{2} \le F_b < 3 \\ \frac{1}{6} & b' = b \;\;\&\;\; 3 \le F_b < 20 \\ 0 & b' = b \;\;\&\;\; 20 \le F_b \\ 0 & b' \ne b \end{cases} \tag{65}$$

$$\frac{\partial C_{b'}}{\partial F_b} = \begin{cases} 0 & b' = b \;\;\&\;\; F_b < 1\frac{1}{2} \\ \frac{2}{3} & b' = b \;\;\&\;\; 1\frac{1}{2} \le F_b < 3 \\ \frac{1}{3} & b' = b \;\;\&\;\; 3 \le F_b < 20 \\ 0 & b' = b \;\;\&\;\; 20 \le F_b \\ 0 & b' \ne b \end{cases} \tag{66}$$

$$\frac{\partial C_{b'}}{\partial F_b} = \begin{cases} 0 & b' = b \;\;\&\;\; F_b < 1\frac{1}{2} \\ \frac{1}{3} & b' = b \;\;\&\;\; 1\frac{1}{2} \le F_b < 3 \\ \frac{1}{6} & b' = b \;\;\&\;\; 3 \le F_b < 20 \\ 0 & b' = b \;\;\&\;\; 20 \le F_b \\ 0 & b' \neq b \end{cases} \tag{67}$$

The next component is the change in differences with respect to the change in SPL. Equation 68 shows how to calculate the differences, including sensitivity, using the 1/3-octave and SPL spectrum, where $\mathrm{L}''_{\mathrm{B},i}$ is determined below and $\mathrm{I}_{b,i'}$ is the identity matrix.

$$\boldsymbol{F} = \mathbf{L}_{\mathrm{B}} - \mathbf{L}''_{\mathrm{B}}, \qquad \frac{\partial F_{b'}}{\partial \mathrm{L}_{\mathrm{B},b}} = \mathrm{I}_{b,b'} - \frac{\partial \mathrm{L}''_{\mathrm{B},b'}}{\partial \mathrm{L}_{\mathrm{B},b}} \tag{68}$$

The term $\mathrm{L}''_{\mathrm{B},b'}$ is an adjusted SPL value which accounts for any tones found within the 1/3-octave band SPL spectrum. It is defined by Eq. 69, with sensitivity defined by Eq. 70.

$$\mathrm{L}''_{\mathrm{B},b} = \begin{cases} \mathrm{N/A} & b \le 2 \\ \mathrm{L}_{\mathrm{B},b} & b = 3 \\ \mathrm{L}''_{\mathrm{B},b-1} + \overline{s}_{b-1} & b > 4 \end{cases} \tag{69}$$

$$\frac{\partial \mathrm{L}''_{\mathrm{B},b'}}{\partial \mathrm{L}_{\mathrm{B},b}} = \begin{cases} \mathrm{N/A} & b' = b \;\;\&\;\; b' \le 2 \\ 1 & b' = b \;\;\&\;\; b' = 3 \\ \dfrac{\partial \mathrm{L}''_{\mathrm{B},b'-1}}{\partial \mathrm{L}_{\mathrm{B},b}} + \dfrac{\partial \overline{s}_{b'-1}}{\partial \mathrm{L}_{\mathrm{B},b}} & b' = b \;\;\&\;\; b' > 4 \\ 0 & b' \neq b \end{cases} \tag{70}$$

The next term is $\overline{s}$, the average slope of the SPL, defined by Eq. 71. Sensitivity of $\overline{s}$ is defined by Eq. 72.

$$\overline{s}_b = \frac{1}{3}(s'_b + s'_{b+1} + s'_{b+2}) \qquad \text{for} \qquad 3 \le b \le 23 \tag{71}$$

$$\frac{\partial \overline{s}_{b'}}{\partial \mathrm{L}_{\mathrm{B},b}} = \frac{1}{3}\left(\frac{\partial s'_{b'}}{\partial \mathrm{L}_{\mathrm{B},b}} + \frac{\partial s'_{b'+1}}{\partial \mathrm{L}_{\mathrm{B},b}} + \frac{\partial s'_{b'+2}}{\partial \mathrm{L}_{\mathrm{B},b}}\right) \qquad \text{for} \qquad b' = b \;\;\&\;\; 3 \le b' \le 23 \tag{72}$$

The definition of s', including an imaginary 25^{th} band, is shown in Eq. 73, with sensitivity shown in

Eq. 74

$$s'_b = \begin{cases} s'_4 & b = 3 \\ L'_{\mathrm{B},b} - L'_{\mathrm{B},b-1} & 3 \le b \le 24 \\ s'_{24} & b = 25 \end{cases} \tag{73}$$

$$\frac{\partial s'_{b'}}{\partial \mathrm{L}_{\mathrm{B},b}} = \begin{cases} \dfrac{\partial s'_4}{\partial \mathrm{L}_{\mathrm{B},b}} & b' = b \;\;\&\;\; b' = 3 \\ \dfrac{\partial \mathrm{L}'_{\mathrm{B},b'}}{\partial \mathrm{L}_{\mathrm{B},b}} - \dfrac{\partial \mathrm{L}'_{\mathrm{B},b'-1}}{\partial \mathrm{L}_{\mathrm{B},b}} & b' = b \;\;\&\;\; 3 \le b' \le 24 \\ \dfrac{\partial s'_{24}}{\partial \mathrm{L}_{\mathrm{B},b}} & b' = b \;\;\&\;\; b' = 25 \\ 0 & b' \ne b \end{cases} \tag{74}$$

$\mathrm{L}'_{\mathrm{B},b}$ is another adjusted SPL value defined on 'encircled' indices. $\mathrm{L}'_{\mathrm{B},b}$ is defined in Eq 75 and its sensitivity in Eq. 76

$$\mathrm{L}'_{\mathrm{B},b} = \begin{cases} \frac{1}{2}(\mathrm{L}_{\mathrm{B},b+1} + \mathrm{L}_{\mathrm{B},b-1}) & \text{encircled } b \\ \mathrm{L}_{\mathrm{B},b} & \text{non-encircled } b \end{cases} \tag{75}$$

$$\frac{\partial \mathrm{L}'_{\mathrm{B},b'}}{\partial \mathrm{L}_{\mathrm{B},b}} = \begin{cases} \frac{1}{2}(\delta_{b(b'+1)} + \delta_{b(b'-1)}) & \text{encircled } b' \\ \delta_{b'b} & \text{non-encircled } b' \end{cases} \tag{76}$$

Encircled $\mathrm{L}'_{\mathrm{B},b}$ values are defined by indices where

(a) If the value of the encircled slope s_b from the previous step is positive and algebraically greater than the slope s_{b-1}, encircle $\mathrm{L}_{\mathrm{B},b}$.

(b) If the value of the encircled slope s_b from the previous step is zero or negative and the slope s_{b-1} is positive, encircle $\mathrm{L}_{\mathrm{B},b-1}$.

(c) For all other cases, no SPL value is to be encircled.

and encircled s_b is indices where $|\Delta s_b|$ is greater than 5

$$|\Delta s_b| = |s_b - s_{b-1}| > 5 \tag{77}$$

and

$$
\begin{aligned}
s_3 &= \text{no value} \\
s_4 &= \mathrm{L_{B,4}} - \mathrm{L_{B,3}} \\
&\ldots \\
s_b &= \mathrm{L_{B,}}_b - \mathrm{L_{B,}}_{b-1} \\
&\ldots \\
s_{24} &= \mathrm{L_{B,24}} - \mathrm{L_{B,23}}
\end{aligned}
\tag{78}
$$

B. Acknowledgments

This work is supported by the NASA Advanced Air Vehicle Program's (AAVP) Revolutionary Vertical Lift Technology (RVLT) Project and the NASA Transformative Aeronautics Concepts Program's (TACP) Transformational Tools and Technologies (TTT) Project. The authors would also like to acknowledge Drs. Boris Diskin and Eric Nielsen for their assistance and discussion of adjoint-based design optimizations.

References

[1]Hill, G. A. and Thomas, R. H., "Challenges and Opportunities for Noise Reduction Through Advanced Aircraft Propulsion Airframe Integration and Configurations," November 2004, 8$^{\text{th}}$ CEAS Workshop on Aeroacoustics of New Aircraft and Engine Configurations.

[2]Collier, F. S., "Environmentally Responsible Aviation (ERA) Project," September 2009, Atlanta, Georgia. NASA Fundamental Aeronautics Program, Third Annual Technical Conference.

[3]Gray, J. S., Moore, K. T., and Naylor, B. A., "OPENMDAO: An Open Source Framework for Multidisciplinary Analysis and Optimization," 13$^{\text{th}}$ AIAA/ISSMO Multidisciplinary Analysis and Optimization Conference, Fort Worth, TX, AIAA Paper 2010-9101, August 2010.

[4]Borggaard, J., Burkardt, J., Gunzburger, M., and Peterson, J., *Optimal Design and Control*, Birkhauser, Boston, 1995.

[5]Yamaleev, N. K., Diskin, B., and Nielsen, E. J., "Adjoint-based Methodology for Time-Dependent Optimization," 12$^{\text{th}}$ AIAA/ISSMO Multidisciplinary Analysis and Optimization Conference, AIAA Paper 2008-5857, September 2008.

[6]Lopes, L. V. and Burley, C. L., "Design of the Next Generation Aircraft NOise Prediction Program: ANOPP2," 17$^{\text{th}}$ AIAA/CEAS Aeroacoustics Conference, AIAA Paper 2011-2854, June 2011.

[7]Lopes, L. V. and Burley, C. L., "ANOPP2 User's Manual," NASA TM-219342, 2016.

[8]Biedron, R. T. and Thomas, J. L., "Recent Enhancements to the FUN3D Flow Solver for Moving Mesh Applications," 47$^{\text{th}}$ AIAA Aerospace Sciences Meeting, AIAA Paper 2009-1360, January 5–8, 2009.

[9]Thomas, P. D. and Lombard, C. K., "Geometrical Conservation Law and Its Application to Flow Computations on Moving Grids," *AIAA Journal*, Vol. 17, No. 10, October 1979, pp. 1030–1037.

[10]Nielsen, E. J. and Diskin, B., "Discrete Adjoint-Based Design for Unsteady Turbulent Flows on Dynamic Overset Unstructured Grids," *AIAA Journal*, Vol. 51, No. 6, June 2013, pp. 1355–1373.

[11]Nielsen, E. J., Diskin, B., and Yamaleev, N. K., "Discrete Adjoint-Based Design Optimization of Unsteady Turbulent Flows on Dynamic Unstructured Grids," *AIAA Journal*, Vol. 48, No. 6, June 2010, pp. 1195–1206.

[12]Biedron, R., Carlson, J., Derlaga, J., Gnoffo, P., Hammond, D., Jones, W., Kleb, B., Lee-Rausch, E., Nielsen, E., Park, M., Rumsey, C., Thomas, J., and Wood, W., "FUN3D Manual: 12.7," NASA TM-218761, 2015.

[13]Lee, S., Brentner, K. S., and Farassat, F., "Analytic Formulation and Numerical Implementation of an Acoustic Pressure Gradient Prediction," *Journal of Sound and Vibration*, Vol. 319, No. 3-5, 2009.

[14]D'Antona, G. and Ferrero, A., *Digital Signal Processing for Measurement Systems*, Springer Media, Inc., New York, 2006.

[15]Cerviño, L. I. and Bewley, T. R., "On the Extension of the Complex-step Derivative Technique to Pseudospectral Algorithms," *Journal of Computational Physics*, Vol. 187, 2003, pp. 544–549.

[16]Acoustical Society of America, "American National Standard Specification for Sound Level Meters," S1.4-1983, 1985.

[17]Acoustical Society of America, "Design Response of Weighting Networks for Acoustical Measurements," S1.42-2001, 1985.

[18]Federal Aviation Administration (FAA), "Noise Standards: Aircraft Type and Airworthiness Certification," AC 36–4C, July 2003.

[19]California Department of Transportation, "Barclay's California Code of Regulations: Noise Standards," Register 2016, Number 16, April 2016.